

TMEM9 promotes intestinal tumorigenesis through vacuolar-ATPase-activated Wnt/ β -catenin signalling

Youn-Sang Jung^{1,8}, Sohee Jun^{1,8}, Moon Jong Kim¹, Sung Ho Lee¹, Han Na Suh¹, Esther M. Lien¹, Hae-Yun Jung¹, Sunhye Lee¹, Jie Zhang¹, Jung-In Yang¹, Hong Ji², Ji Yuan Wu³, Wenqi Wang⁴, Rachel K. Miller^{2,5,6,7}, Junjie Chen^{1,6,7}, Pierre D. McCreary^{2,6,7}, Scott Kopetz³ and Jae-Il Park^{1,6,7*}

Vesicular acidification and trafficking are associated with various cellular processes. However, their pathologic relevance to cancer remains elusive. We identified transmembrane protein 9 (TMEM9) as a vesicular acidification regulator. TMEM9 is highly upregulated in colorectal cancer. Proteomic and biochemical analyses show that TMEM9 binds to and facilitates assembly of vacuolar-ATPase (v-ATPase), a vacuolar proton pump, resulting in enhanced vesicular acidification and trafficking. TMEM9-v-ATPase hyperactivates Wnt/ β -catenin signalling via lysosomal degradation of adenomatous polyposis coli (APC). Moreover, TMEM9 transactivated by β -catenin functions as a positive feedback regulator of Wnt signalling in colorectal cancer. Genetic ablation of TMEM9 inhibits colorectal cancer cell proliferation in vitro, ex vivo and in vivo mouse models. Moreover, administration of v-ATPase inhibitors suppresses intestinal tumorigenesis of APC mouse models and human patient-derived xenografts. Our results reveal the unexpected roles of TMEM9-controlled vesicular acidification in hyperactivating Wnt/ β -catenin signalling through APC degradation, and propose the blockade of TMEM9-v-ATPase as a viable option for colorectal cancer treatment.

Wnt signalling orchestrates development, tissue homeostasis and tissue regeneration¹. However, deregulation of Wnt signalling is highly associated with cancers². In the absence of Wnt ligand, a protein destruction complex, glycogen synthase kinase 3 (GSK3), adenomatous polyposis coli (APC), Axin and CK1, phosphorylates β -catenin for ubiquitin-mediated degradation. Conversely, the binding of Wnt ligand to Frizzled receptor and low-density lipoprotein-receptor related protein (LRP5/6) co-receptor triggers the recruitment of Dishevelled (Dvl) and Axin to the plasma membrane^{1,3,4}. The ligand-receptor interaction induces the formation of the LRP signalosome (phosphorylated LRP6, Frizzled, Dvl, Axin and GSK3)³. Subsequently, the LRP signalosome inhibits GSK3, which stabilizes the β -catenin protein. Then, stabilized (activated) β -catenin protein is translocated into the nucleus and transactivates its downstream target genes, in association with its nuclear partners, T-cell factor (TCF)/lymphoid enhancer factor 1 (LEF)^{1,5}. It has also been proposed that the sequestration of GSK3 into the multivesicular body (MVB) inhibits cytosolic GSK3 kinase activity and activates β -catenin⁶. Genetic mutations in the core components of Wnt/ β -catenin signalling lead to the initiation of intestinal tumorigenesis⁷. Accumulating evidence suggests that additional factors complement Wnt signalling activity in colorectal cancer (CRC)^{8–11}. Therefore, beyond genetic mutations in Wnt signalling core components, further layers of Wnt signalling regulation probably contribute to intestinal tumorigenesis.

Vesicular acidification and trafficking play key roles in cell physiology^{12,13}. However, their contribution to cancer remains unknown. Here, we identified transmembrane protein 9 (TMEM9) as a regulator of vesicular acidification in CRC. We found that TMEM9 promotes vesicular acidification via vacuolar adenosine triphosphatase (v-ATPase). v-ATPase is an ATP-dependent proton pump for intracellular compartment acidification^{14,15}. v-ATPase is a multisubunit protein complex composed of membrane-bound (V0) subunits (a, c, c', d, e, ATP6AP1) and cytosolic (V1) subunits (A–H). The V1 subunits catalyse ATP hydrolysis for the proton pump through V0 subunit complex. ATP6AP2 (also known as prorenin receptor), an accessory protein of v-ATPase, has been shown to transduce both canonical and non-canonical Wnt signals^{16–18}. Herein, we investigated how deregulated vesicular acidification contributes to CRC.

Results

Expression of TMEM9 in CRC. To identify genes playing crucial roles in intestinal tumorigenesis, we analysed publicly available gene expression data sets, and selected genes highly expressed in CRC compared with normal tissues. We chose *TMEM9* as a gene potentially associated with intestinal tumorigenesis. *TMEM9* contains a signal peptide (SP) and one transmembrane domain (TMD) (Fig. 1a). OncoPrint analysis showed that *TMEM9* was markedly upregulated in CRC and breast cancer (Fig. 1b). *TMEM9* is also highly expressed in CRC cells, compared to normal intestinal epithelial cells (IECs) (Fig. 1c). Additionally, quantitative reverse

¹Department of Experimental Radiation Oncology, The University of Texas MD Anderson Cancer Center, Houston, TX, USA. ²Department of Genetics, The University of Texas MD Anderson Cancer Center, Houston, TX, USA. ³Department of Gastrointestinal Medical Oncology, The University of Texas MD Anderson Cancer Center, Houston, TX, USA. ⁴Department of Developmental and Cell Biology, University of California, Irvine, Irvine, CA, USA. ⁵Department of Pediatrics, The University of Texas McGovern Medical School, Houston, TX, USA. ⁶Graduate School of Biomedical Sciences at Houston, The University of Texas Health Science Center and MD Anderson Cancer Center, Houston, TX, USA. ⁷Program in Genes and Epigenetics, The University of Texas MD Anderson Cancer Center, Houston, TX, USA. ⁸These authors contributed equally: Youn-Sang Jung and Sohee Jun. *e-mail: jaeil@mdanderson.org

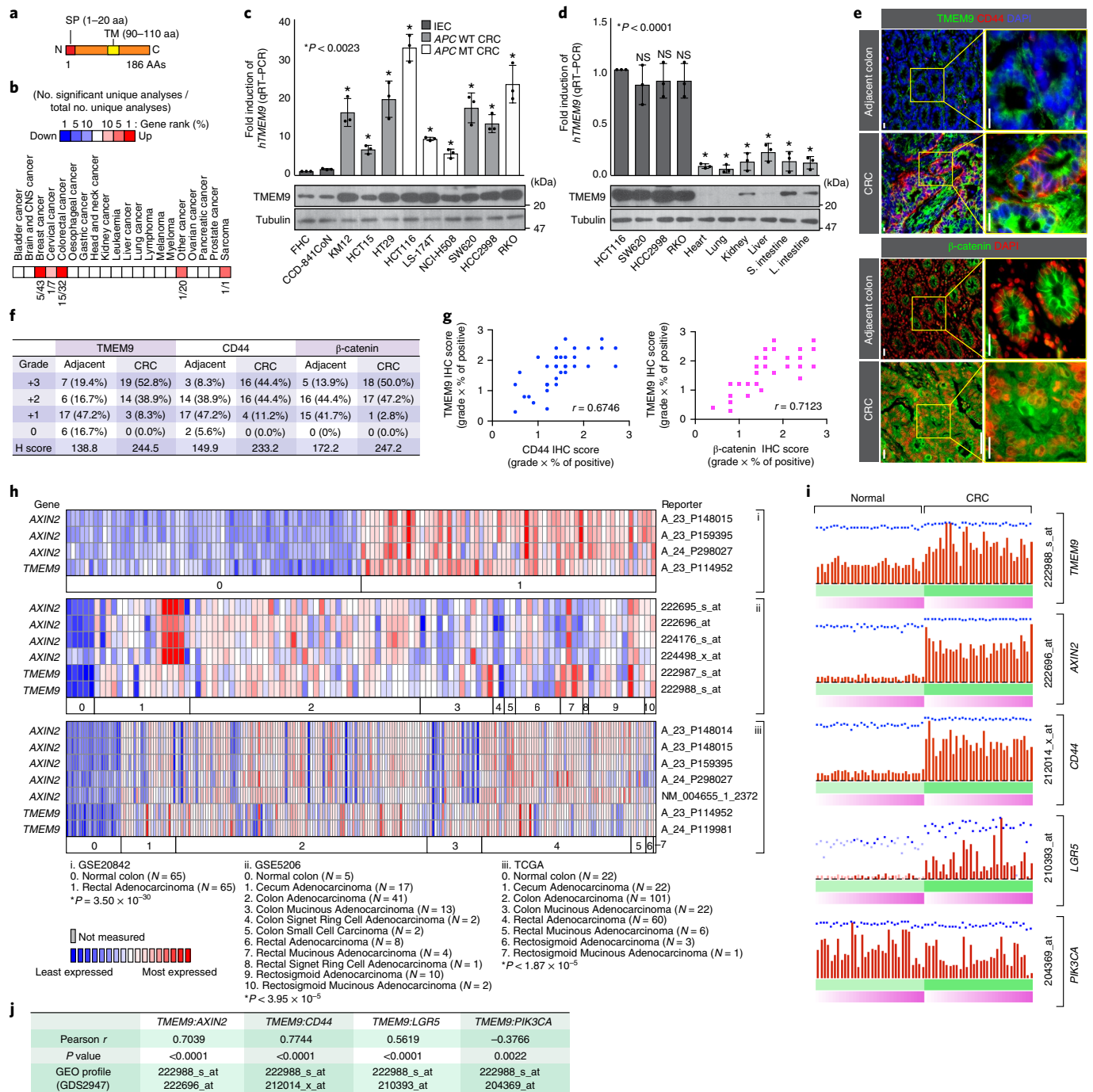


Fig. 1 | Expression of TMEM9 in CRC cells. **a**, Illustration of the TMEM9 domains. **b**, In silico analysis of *TMEM9* expression in CRC. OncoPrint analysis of *TMEM9* expression in human cancers (www.oncoPrint.org). 10% gene rank; $P < 0.0001$; fold change > 2 ; compared with normal cells. **c**, High expression of *TMEM9* in CRC. Two IECs and nine CRC cells were collected for IB and qRT-PCR. Tubulin served as a loading control, and *TMEM9* expression was normalized by *HPRT1*. $n = 3$ independent experiments. **d**, Expression of *TMEM9* in mouse tissues. Protein and mRNAs were extracted from six mouse tissues and assessed by IB and qRT-PCR. CRC cells served as a positive control. $n = 3$ independent experiments. **e-g**, Expression of *TMEM9*, *CD44* and β -catenin in CRC TMA: IHC of *TMEM9*, *CD44* and β -catenin was performed using TMA (Biomax, BC05023) (**e**), and H score (**f**) and Pearson's correlations (**g**) were calculated. $n = 36$ biologically independent samples. **h**, Co-expression of *TMEM9* with *AXIN2*. OncoPrint analysis of GSE20842, GSE5206 and TCGA data sets; 10% gene rank; $P < 0.0001$; fold change > 2 ; compared with normal cells. **i, j**, Co-expression of *TMEM9* with Wnt/ β -catenin target genes. GEO data sets (GDS2947) were analysed for each gene expression in normal intestine and matched CRC samples (32 patient samples, **i**). Pearson's correlations were determined (**j**). Scale bars, 20 μ m; NS, not significant. Error bars represent mean \pm s.d. Two-sided unpaired t -test.

transcriptase PCR (qRT-PCR) assays and immunoblotting (IB) showed that *TMEM9* expression in CRC was much higher than in other tissues (Fig. 1d). Immunohistochemistry (IHC) of tumour

microarrays (TMAs) validated the upregulation of *TMEM9* in CRC patient samples, whereas it was barely expressed in normal intestinal crypts (Fig. 1e,f). Given the pivotal roles of Wnt

signalling in CRC, we examined whether *TMEM9* is co-expressed with β -catenin and its target gene (*CD44*)¹⁹. IHC results showed the positive correlation between *TMEM9* and both β -catenin and *CD44* (Fig. 1g). Moreover, multiple gene expression data sets indicated the upregulation of both *TMEM9* and *AXIN2* in CRC (Fig. 1h and Supplementary Table 1). Similarly, *GDS2947* data sets in the Gene Expression Omnibus showed the significant upregulation and positive correlation of *TMEM9* and Wnt signalling-associated genes (*AXIN2*, *CD44*, *LGR5*) in CRC, compared to adjacent normal samples (Fig. 1i,j). These results suggest that *TMEM9* is highly expressed in CRC with hyperactivation of β -catenin and its target genes.

Activation of Wnt/ β -catenin signalling by *TMEM9* in vitro and in vivo. To understand the pathologic impacts of *TMEM9* upregulation to intestinal tumorigenesis, we examined the effects of *TMEM9* depletion on CRC-related cellular signalling. HCT116 CRC cells stably expressing shRNAs against *TMEM9* displayed the downregulation of Wnt signalling target genes (*AXIN2*, *CD44*), while other signalling pathways were barely affected (Fig. 2a and Supplementary Fig. 1a,b). Conversely, ectopic expression of *TMEM9* in IECs upregulated Wnt targets (Fig. 2b, and Supplementary Fig. 1c). These results imply that *TMEM9* might be associated with Wnt/ β -catenin signalling, which led us to hypothesize that *TMEM9* positively modulates Wnt/ β -catenin signalling. To test this, we analysed the effects of *TMEM9* on the β -catenin protein. Immunofluorescent (IF) staining showed that *TMEM9* expression increased both cytosolic and nuclear β -catenin (Fig. 2c). Consistently, *TMEM9* overexpression increased the half-life of β -catenin protein (Fig. 2d and Supplementary Fig. 1d). Additionally, β -catenin reporter (TOPFLASH) and qRT-PCR assays showed that *TMEM9* expression per se enhanced the transcriptional activity of β -catenin (Fig. 2e and Supplementary Fig. 1e,f). Intriguingly, *TMEM9* increased the response of β -catenin reporter activation by LiCl, a GSK3 inhibitor (Fig. 2f). Similarly, *TMEM9* also enhanced β -catenin protein stabilization induced by Wnt3a (Fig. 2g). Additionally, iCRT14, an inhibitor of β -catenin-TCF binding, suppressed *TMEM9*-activated luciferase activity (Fig. 2h). To complement gain-of-function assays, we also utilized shRNAs to deplete endogenous *TMEM9* (Supplementary Fig. 1g). Based on the high expression of *TMEM9* in CRC cell lines (Fig. 1c,d), we used CRC cells for knockdown experiments. *TMEM9*-depleted HCT116 cells displayed a decrease in β -catenin protein as well as active β -catenin (Fig. 2i). Next, we examined the effects of *TMEM9* knockdown on β -catenin's transcriptional activity. qRT-PCR and β -catenin reporter assays showed that *TMEM9* depletion downregulated *AXIN2* and β -catenin reporter activity in CRC cells (Fig. 2j,k and Supplementary Fig. 1h,i). Of note, *TMEM9* depletion-induced *AXIN2* downregulation was rescued by ectopic expression of β -catenin (Fig. 2l), suggesting that β -catenin mediates the effect of *TMEM9* on *AXIN2* upregulation. Consistently, similar effects were observed in *TMEM9* knockout (KO) HCT116 cells (Fig. 2m and Supplementary Fig. 1j,k). Next, to better understand the epistasis of *TMEM9* in Wnt signalling, we assessed the effects of *TMEM9* depletion on β -catenin-mediated transactivation by Dvl2 and Wnt3a. We found that *TMEM9* knockdown diminished both Dvl2- and Wnt3a-induced β -catenin reporter activation (Fig. 2n), implying that *TMEM9* might activate Wnt signalling at the same or downstream level of Wnt ligands and Dvls. We also examined the *in vivo* effects of *TMEM9* on Wnt signalling by axis duplication assays using *Xenopus laevis* embryos. Ectopic activation of Wnt/ β -catenin signalling in ventro-vegetal blastomeres generates a secondary anterior-posterior axis²⁰ (Fig. 2o). We observed that ventro-vegetal microinjection of *xTMEM9* or *x β -catenin* (positive control) mRNA induced the additional anterior-posterior axis (Fig. 2p-r). These results suggest that *TMEM9* activates Wnt signalling *in vitro* and *in vivo*.

***TMEM9* binds and activates v-ATPase by promoting v-ATPase-ATP6AP2 assembly.** To elucidate the molecular mechanism of *TMEM9*-activated Wnt/ β -catenin signalling, we sought to identify *TMEM9*-interacting proteins using tandem affinity protein purification and mass spectrometry analysis (TAP-MS/MS) (Fig. 3a). Interestingly, we identified that *TMEM9* was highly associated with the v-ATPase protein components ATP6AP2, a v-ATPase accessory protein, and ATP6V0D1, a rotary subunit mediating V0-V1 coupling¹⁴. ATP6AP2 has previously been shown to connect the LRP signalosome to v-ATPase¹⁶. Thus, we hypothesized that *TMEM9* modulates v-ATPase activity through physical interaction with v-ATPase and ATP6AP2. Co-immunoprecipitation (co-IP) assays confirmed that *TMEM9* bound to both ATP6AP2 and ATP6V0D1 in 293T (Fig. 3b,c) and CRC cells (Fig. 3d and Supplementary Fig. 2a). However, unlike the previous study¹⁶, *TMEM9* did not bind to LRP signalosome components (Fig. 3e,f), consistent with our proteomic analysis (Fig. 3a). Based on *TMEM9*'s SP and TMD, we also tested whether *TMEM9*'s membrane targeting is required for interaction with either ATP6V0D1 or ATP6AP2. Co-IP for either wild-type (WT) or a Δ TMD mutant (MT) of *TMEM9* showed that *TMEM9*'s TMD is essential for interacting with ATP6AP2 (Fig. 3g), but not with ATP6V0D1 (Fig. 3h). ATP6V0D1 functions as a central stalk that regulates v-ATPase assembly²¹. Additionally, ATP6AP2 is indispensable for v-ATPase assembly²². Thus, modulating the interaction between ATP6AP2 and v-ATPase might affect the activity of v-ATPase. To test this, we asked whether *TMEM9* promotes v-ATPase assembly. Co-IP assays showed that *TMEM9* expression enhanced ATP6AP2-ATP6V0D1 interaction in 293T cells (Fig. 3i). Conversely, *TMEM9* depletion decreased ATP6AP2-ATP6V0D1 binding in HCT116 cells (Fig. 3j). Next, we assessed the effects of *TMEM9* on v-ATPase activity. We performed co-IP experiments using ATP6AP2 antibody in HeLa (Control vector (Vec) versus *TMEM9* expressing) cells and quantified ATP6AP2-associated ATPase activity by measuring inorganic phosphate (P_i) released by ATP hydrolysis. Co-immunoprecipitates of ATP6AP2 from HeLa-*TMEM9* displayed a markedly increased level of P_i following ATP addition, compared with those from control (Fig. 3k). These results suggest that *TMEM9* positively modulates v-ATPase activity. Additionally, amino acid sequence analysis located a dimerization motif ([G/S/A/L/I]-XXX-[G/S/A/L/I])²³ in the TMD of *TMEM9* (Fig. 3l). Co-IP assays showed that different epitope-tagged *TMEM9* proteins bound to each other, implying the potential oligomerization of *TMEM9* (Supplementary Fig. 2b). Also, binding domain-mapping analysis suggests that the N terminus of *TMEM9* is required for binding to ATP6AP2 (Fig. 3m).

TMEM9 contains an SP and one α -helix TMD (Fig. 1a), implying its possible localization to membranous organelles and/or the plasma membrane. IF staining showed that both endogenous and exogenous *TMEM9* localized to the cytoplasm and the perinucleus with a speckled pattern in HCT116 and HeLa cells (Fig. 3n and Supplementary Fig. 2c), consistent with the results from CRC tissue immunostaining (Fig. 1e). Co-IF showed that *TMEM9* mainly co-localized with LAMP1, a marker for the MVB (Fig. 3o). The lower pH in the lumen of membranous organelles is maintained by v-ATPase-mediated proton efflux. Given the subcellular localization of *TMEM9* in the MVB (Fig. 3o) and *TMEM9*-activated v-ATPase (Fig. 3k), we tested whether *TMEM9* increases intracellular vesicle acidification, using LysoTracker, a marker for acidic organelles. Depletion of *TMEM9* significantly decreased vesicle acidification (Fig. 3p and Supplementary Fig. 2d), while *TMEM9* expression increased it (Fig. 3q and Supplementary Fig. 2e). To validate the effects of *TMEM9* on vesicular acidification, we utilized bafilomycin A1 (BAF), an inhibitor of v-ATPase²⁴. BAF inhibited *TMEM9*-induced vesicular acidification (Fig. 3q). These results suggest that *TMEM9* binds to ATP6AP2 and v-ATPase, and increases v-ATPase activity, which results in the vesicular acidification (Fig. 3r).

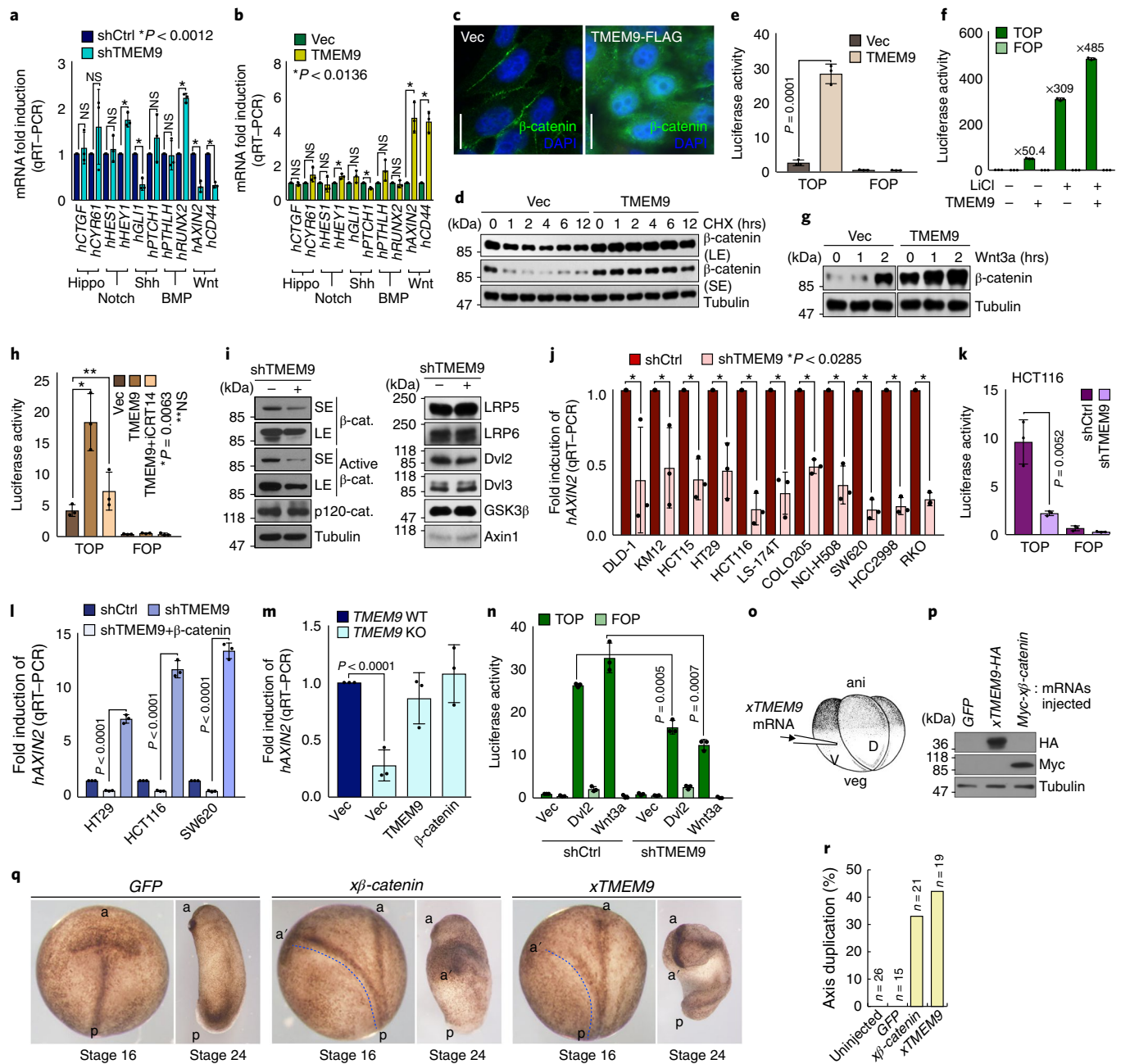


Fig. 2 | Activation of Wnt/β-catenin signalling by TMEM9. **a, b**, Screening of cell signalling. mRNA expression in CRC cells (**a**) and IECs (**b**) was analysed by qRT-PCR. **c, d**, Upregulation of β-catenin by TMEM9: IF staining of β-catenin (**c**); HeLa cells were analysed for β-catenin protein half-life using cycloheximide (CHX; 100 μg ml⁻¹) (**d**). **e, f**, Activation of the β-catenin reporter by TMEM9: CCD-841CoN cells were analysed by β-catenin reporter luciferase assays (TOPFLASH (TOP) and FOPFLASH (FOP)) (**e**); 293T cells were transfected with each plasmid and treated with LiCl (25 mM, 24 h) (**f**). **g**, Enhancement of β-catenin stabilization by TMEM9 upon Wnt3a. IB of 293T cells transiently expressing Ctrl or TMEM9 upon Wnt3a treatment (200 ng ml⁻¹). **h**, Decreased TMEM9-activated β-catenin reporter by iCRT14. At 48 h after overexpression of TMEM9, CCD-841CoN cells were incubated with vehicle or iCRT14 (100 μM, 12 h). **i**, Inhibition of β-catenin by TMEM9 depletion. IB of HCT116 (shCtrl versus shTMEM9). **j, k**, Decreased β-catenin transcription activity by shTMEM9: qRT-PCR of *AXIN2* (**j**) and luciferase activity of TOP/FOP (**k**). **l, m**, Rescue of Wnt/β-catenin activity by ectopic expression of β-catenin in TMEM9-depleted CRC. CRC cells were transfected with indicated plasmids for 24 h (**l**). HCT116 (TMEM9 WT versus KO) cells were stably transduced with either TMEM9 or β-catenin (**m**). **n**, Wnt/β-catenin signalling activation by TMEM9 at the downstream of Dvl2 and Wnt3a. HCT116 cells were co-transfected with β-catenin reporter plasmids and Dvl2 or treated with Wnt3a for luciferase assays. **o–r**, In vivo activation of Wnt/β-catenin signalling by *xTMEM9* in frog embryos. *X. laevis* embryos were injected with each mRNA into ventral-vegetal blastomeres at the four-cell stage (**o**). Expression of microinjected *Myc-xβ-catenin* or *xTMEM9-HA* mRNA was confirmed by IB (**p**). Axis duplication was analysed at the neural fold (st16) and the tail buds (st24) stages (**q**). Quantification of axis duplication (**r**). ani, animal pole; veg, vegetal pole; V, ventral region; D, dorsal region; a, anterior; p, posterior; a', secondary anterior axis; n, biologically independent samples. The experiment was performed once. Images in **c** and blots in **d, g, i** and **p** are representative of three independent experiments with similar results; Scale bars, 20 μm; LE, long exposure; SE, short exposure; NS, not significant; Error bars indicate mean ± s.d.; two-sided unpaired t-test.

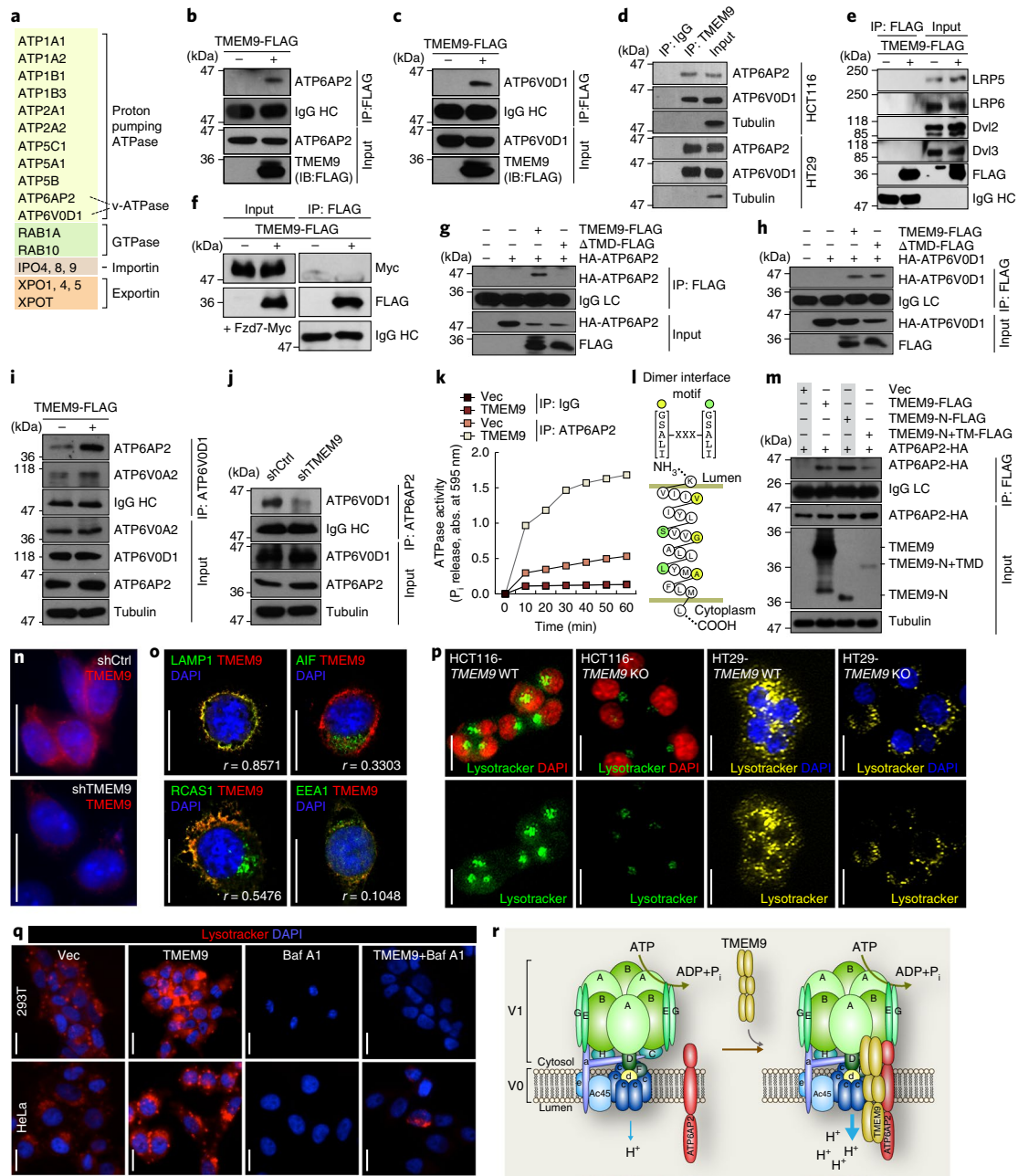


Fig. 3 | TMEM9 facilitates assembly of v-ATPase. **a**, Identification of TMEM9-interacting proteins. 293T cells stably expressing TMEM9 were processed for TAP-MS/MS. The experiment was performed once. **b,c**, Interaction of TMEM9 with v-ATPase components ATP6AP2 (**b**) and ATP6V0D1 (**c**). 293T cells were transfected with each plasmid and analysed for co-IP. HC, heavy chain; LC, light chain. **d**, Endogenous binding of TMEM9 to ATP6AP2 and ATP6V0D1. Co-IP of HCT116 and HT29. **e,f**, No interaction of TMEM9 with LRPs, Dvls and Fzd. Co-IP of 293T cells transfected with TMEM9-FLAG plasmids (**e**) or co-transfected with TMEM9-FLAG and Fzd7-Myc plasmids (**f**). **g,h**, Requirement of TMEM9-TMD for binding to ATP6AP2 but not ATP6V0D1. 293T cells were transfected with each plasmid and analysed by co-IP. **i**, Increased ATP6AP2-ATP6V0D1 binding by TMEM9. 293T stable cells (Ctrl versus TMEM9) were analysed by co-IP. **j**, Decreased ATP6AP2-ATP6V0D1 binding by TMEM9 depletion. HCT116 stable cells (shCtrl versus shTMEM9) were analysed by co-IP. **k**, Upregulation of ATP6AP2-associated ATPase activity by TMEM9. HCT116 cells were immunoprecipitated using ATP6AP2 antibody. The immunoprecipitates were then analysed for ATPase activity. The experiment was performed twice with similar results ($n=3$ each independent samples). **l**, Illustration of TMD of TMEM9 using TOPO2 (<http://www.sacs.ucsf.edu/cgi-bin/open-topo2.py>). **m**, Binding of ATP6AP2 to the N terminus of TMEM9. 293T cells were transfected with each TMEM9 mutant plasmid and analysed by co-IP. **n**, Subcellular localization of endogenous TMEM9. IF staining of HCT116 (shCtrl versus shTMEM9). **o**, Localization of TMEM9 in the MVBs. Co-IF staining of TMEM9 with organelle markers in HCT116 cells. AIF, mitochondria; EEA1, early endosome; LAMP1, MVB; RCAS1, Golgi complex. Quantification of co-localization was performed using ImageJ. **p**, Downregulation of MVB acidification by TMEM9 KO in vitro. HCT116 and HT29 (TMEM9 WT versus KO) cells were stained with LysoTracker (30 min). **q**, TMEM9-induced vesicle acidification via v-ATPase. 293T and HeLa cells stably expressing Ctrl vector or TMEM9 were treated with BAF (10 nM, 24 h), and stained with LysoTracker. **r**, Schematic illustration of TMEM9-induced activation of v-ATPase. TMEM9 promotes interaction between v-ATPase and ATP6AP2, which leads to activation of v-ATPase. V1, cytosolic units hydrolysing ATP; V0, membrane-bound subunits. Images are representative of three experiments with similar results (blots of **b-j** and **m**; images of **n-q**). Scale bars, 20 μ m.

Activation of Wnt/ β -catenin signalling by TMEM9-v-ATPase-mediated APC degradation. We next questioned whether v-ATPase is required for TMEM9-induced Wnt signalling activation. Recent studies have proposed a crucial role of MVBs in transducing Wnt signalling^{3,16}. Given (1) the localization of TMEM9 to MVBs (Fig. 3o), (2) co-expression of *TMEM9* with β -catenin target genes in CRC (Fig. 1e–j), (3) TMEM9-activated Wnt/ β -catenin signalling (Fig. 2) and (4) TMEM9-enhanced v-ATPase activity (Fig. 3), we hypothesized that TMEM9-induced vesicular acidification activates Wnt/ β -catenin signalling. We found that blockade of v-ATPase using BAF suppressed TMEM9-induced β -catenin protein stabilization (Supplementary Fig. 3a,b). Additionally, TMEM9-activated β -catenin reporter was suppressed by BAF or concanamycin A (CMA), another v-ATPase inhibitor²⁴ (Fig. 4a). Additionally, Δ TMD-TMEM9 was unable to activate β -catenin reporter activity (Fig. 4b,c and Supplementary Fig. 3c,d), indicating that TMEM9's membrane targeting is necessary for Wnt signalling activation. We also observed that ATP6AP2 depletion inhibited TMEM9-induced Wnt signalling activation (Supplementary Fig. 3e,f), suggesting that ATP6AP2 is required for TMEM9-activated Wnt signalling. We further tested whether TMEM9 and ATP6AP2 are reciprocally dependent in activating Wnt signalling. TMEM9 depletion-reduced Wnt/ β -catenin signalling activity was not restored by ATP6AP2 and vice versa (Fig. 4d,e and Supplementary Fig. 3g,h), unlike β -catenin, a positive control (Supplementary Fig. 3i,j).

MVB acidification activates FZD/LRP6-dependent Wnt/ β -catenin signalling¹⁶. Thus, we tested whether TMEM9 affects FZD/LRP6-mediated Wnt signalling activation. We found that TMEM9-activated Wnt/ β -catenin signalling was not affected by Dkk-1, a Wnt antagonist (Fig. 4f and Supplementary Fig. 3k). Moreover, TMEM9 depletion inhibited Wnt/ β -catenin signalling, independently of Wnt3a (Fig. 4g and Supplementary Fig. 3l). Although it was proposed that MVB increases the secretion of Wnt ligands^{25,26}, TMEM9-depletion-downregulated Wnt/ β -catenin signalling was not affected by porcupine inhibitor, IWP-2 (Fig. 4h and Supplementary Fig. 3m).

It was recently shown that mutant APC still induces β -catenin degradation¹⁰. Having determined that TMEM9 depletion inhibits Wnt/ β -catenin signalling regardless of APC mutation (Fig. 2j,k and Supplementary Fig. 1h,i), we tested whether TMEM9-induced MVB acidification alters APC protein level. Interestingly, *TMEM9* KO and shTMEM9 cells showed an increase in APC protein (Fig. 4i and Supplementary Fig. 3n). v-ATPase inhibitors also increased APC protein with decreased β -catenin in both HCT116 (APC WT; 2,843 amino acids) and HT29 (APC MT; 1,555 amino acids)^{10,27} cells, while hydroxychloroquine (HCQ), an inhibitor of autophagy, did not (Fig. 4j). Vesicular acidification is indispensable for lysosomal protein degradation²⁸. Thus, we determined whether lysosomal protein degradation mediates TMEM9-depletion-increased APC protein. We found that inhibition of cathepsin, a lysosomal protease, increased both WT and MT APC protein along with the decreased β -catenin (Fig. 4k). Next, we asked whether APC mediates TMEM9-depletion-induced β -catenin downregulation using APC KO cells. shTMEM9 showed no decrease in β -catenin protein and *AXIN2* expression in APC KO-HCT116 and -HT29 cells (Fig. 4l–o). We also found that β -catenin bound to both WT and MT APC, which was increased by *TMEM9* KO (Fig. 4p–s). Similarly, BAF also increased the APC– β -catenin interaction (Fig. 4r,s). These results suggest that the TMEM9-v-ATPase axis activates Wnt/ β -catenin signalling by lysosomal degradation of APC.

Transactivation of *TMEM9* by β -catenin. Next, we sought to understand how TMEM9 is upregulated in CRC. Having observed the co-expression of *TMEM9* with β -catenin targets in CRC (Fig. 1e–j), we tested whether Wnt/ β -catenin signalling upregulates *TMEM9* in CRC. Interestingly, iCRT14-treated HCT116 exhibited downregulation of *TMEM9* transcripts (Fig. 5a) and protein (Fig. 5b).

Similarly, Engrailed- Δ N-LEF1 (Eng-LEF1), a dominant-negative MT for β -catenin-mediated transcription²⁹, also downregulated TMEM9 (Fig. 5c). Conversely, Wnt3a upregulated TMEM9 in 293T cells (Fig. 5d). Additionally, β -catenin ectopic expression upregulated TMEM9 (Fig. 5e,f), which was inhibited by Eng-LEF1 (Fig. 5f). In silico analysis identified the potential TCF/LEFs binding elements (TBEs; CTTTGA/TA/T) in conserved non-coding sequences (CNSs) between human and mouse *TMEM9* promoter (Fig. 5g), which led us to test whether β -catenin directly transactivates *TMEM9*, using chromatin immunoprecipitation (ChIP) assays. ChIP for endogenous β -catenin showed that β -catenin occupied the proximal promoter of *TMEM9* in HCT116 cells (Fig. 5h). Given that *TMEM9* is upregulated by Wnt signalling activation (Fig. 5d–f), we also asked whether β -catenin conditionally occupies the *TMEM9* promoter following Wnt signalling activation. Indeed, in the setting of treatment of LiCl, β -catenin occupied the *TMEM9* promoter (Fig. 5i). Next, we examined whether β -catenin upregulates *TMEM9* in vivo. Both *TMEM9* mRNA and protein levels were highly increased in intestinal adenomas of *APC^{MIN}* mice (Fig. 5j,k). These results suggest that β -catenin directly transactivates *TMEM9* in CRC.

Suppression of intestinal tumorigenesis by TMEM9 blockade. Our results showed (1) specific upregulation of TMEM9 in CRC and (2) TMEM9-activated Wnt/ β -catenin signalling. Moreover, the Kaplan–Meier plot of human CRC showed lower survival with high expression of *TMEM9* (Supplementary Fig. 4a). These data prompted us to hypothesize that TMEM9 plays key roles in intestinal tumorigenesis. To test this, we assessed the effects of TMEM9 depletion on CRC cell proliferation (shCtrl versus shTMEM9). We found that TMEM9-depleted CRC cells displayed decreased cell growth (Fig. 6a–c and Supplementary Fig. 4b,c) without a change in cell death (Fig. 6d), which was rescued by β -catenin expression (Fig. 6e). These results suggest that β -catenin mediates TMEM9's mitogenic effect on CRC cells.

To gain further insights into the tumorigenic roles of TMEM9 in more physiological settings, we subcutaneously injected TMEM9-depleted CRC cells into immunocompromised mice and analysed for tumour formation. TMEM9-depleted CRC cells developed smaller tumours (Fig. 6f,g and Supplementary Fig. 4d,e) with decreased cell proliferation (Ki67) and downregulated CD44 (Supplementary Fig. 4f).

To complement the ex vivo results, we established *TMEM9* KO mice (Fig. 6h and Supplementary Fig. 4g). *TMEM9* KO mice were viable without any apparent phenotype (Fig. 6i,j and Supplementary Fig. 4h). To determine whether *TMEM9* KO suppresses intestinal tumorigenesis, we generated *APC^{MIN}:TMEM9^{-/-}* compound strains. *APC^{MIN}* mice die with multiple adenomas in the small intestine³⁰. While the median survival of *APC^{MIN}* mice was 124 days of age, that of *APC^{MIN}:TMEM9^{-/-}* mice was 323 days. Of note, heterozygous KO of *TMEM9* (*APC^{MIN}:TMEM9^{+/-}*) was also sufficient to increase survival (median survival: 199 days; Fig. 6i and Supplementary Fig. 4i). We also monitored the tumour size and number of *APC^{MIN}*-, *APC^{MIN}:TMEM9^{+/-}*- and *APC^{MIN}:TMEM9^{-/-}*-induced tumours at three months of age. Although *TMEM9* KO slightly decreased tumour size (Fig. 6k), tumour number was significantly reduced compared to *TMEM9* WT (Fig. 6l). qRT-PCR and IHC analyses showed a decreased transcriptional activity (Fig. 6m) and protein level of β -catenin (Fig. 6n,o), diminished β -catenin target expression (cyclin D1, CD44; Fig. 6n and Supplementary Fig. 4j) and reduced cell proliferation (Fig. 6q,r), compared to *APC^{MIN}* mice. Of note, the number of nuclear β -catenin-positive cells in tumours was decreased in *APC^{MIN}:TMEM9^{-/-}* mice (Fig. 6o,p) without a significant difference in apoptosis (c-Cas3; Supplementary Fig. 4k) and epithelial–mesenchymal transition (EMT; Supplementary Fig. 4l,m). These results strongly suggest that genetic ablation of *TMEM9* suppresses intestinal tumorigenesis ex vivo and in vivo.

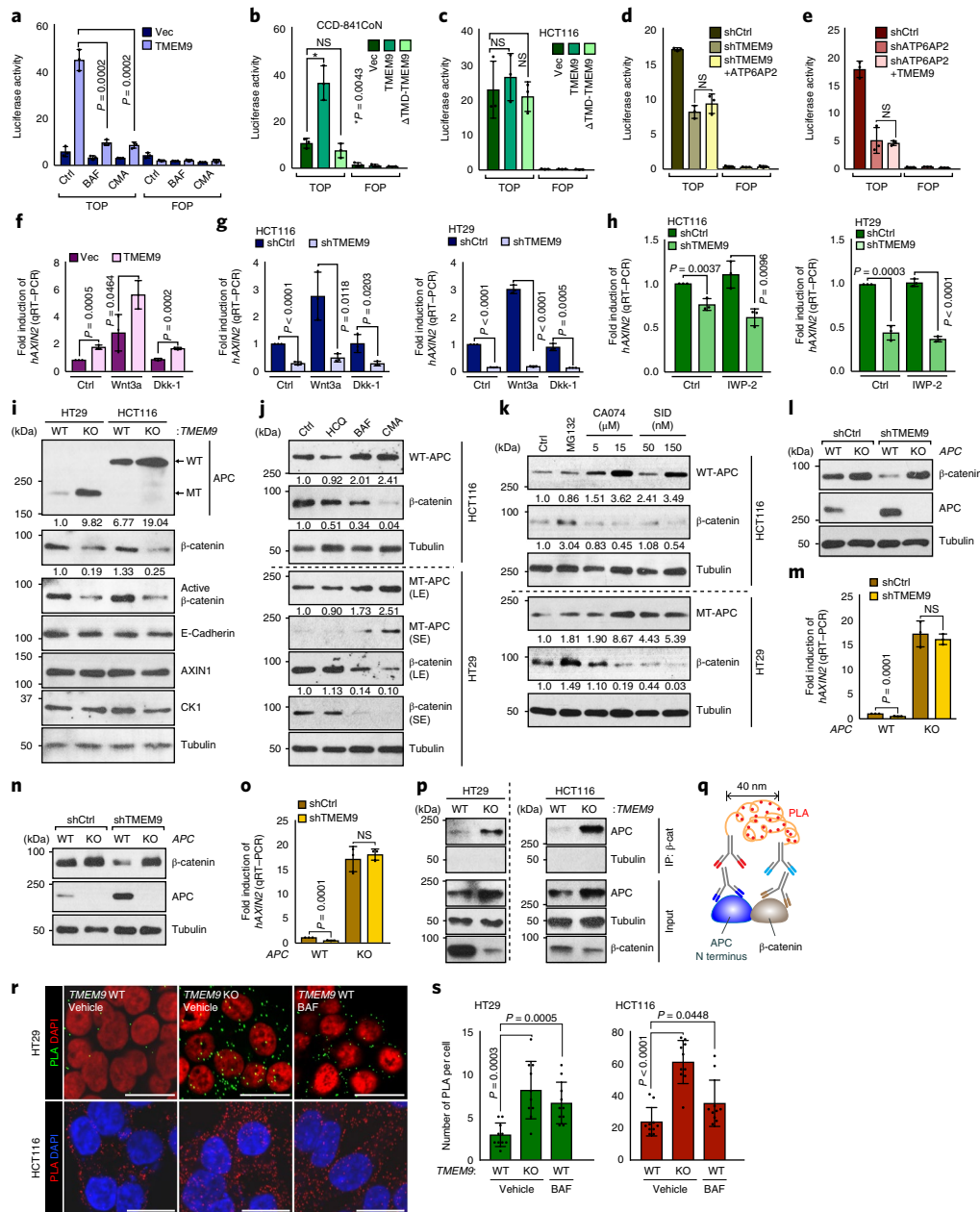


Fig. 4 | Decrease of APC by TMEM9-induced v-ATPase activation. **a**, Suppression of TMEM9-activated β -catenin reporter by v-ATPase inhibitors. 239T cells were transfected with β -catenin reporter plasmids and treated with BAF or CMA for 24 h. **b,c**, Requirement of TMEM9-TMD for TMEM9-induced β -catenin reporter activation; CCD-841CoN (**b**) and HCT116 (**c**) cells were transfected with indicated plasmids and analysed by luciferase assays. **d,e**, No effect of ATP6AP2 and TMEM9 on β -catenin reporter activity in TMEM9- or ATP6AP2-depleted CRC cells, respectively: shCtrl, shTMEM9 (**d**) or shATP6AP2 (**e**) plasmids were co-transfected with ATP6AP2 (**d**) or TMEM9 (**e**) plasmids, respectively. **f,g**, Increased β -catenin transcription activity by TMEM9 independently of Wnt agonist or antagonist: IECs (**f**) and CRC cells (**g**) were incubated with Wnt3a (50 ng ml⁻¹) or Dkk-1 (100 ng ml⁻¹) for 12 h and analysed by *AXIN2* qRT-PCR. **h**, Downregulation of Wnt/ β -catenin signalling by shTMEM9 independently of Wnt ligand secretion. After transfection, cells were incubated with IWP-2 (2 μ M) for 12 h. qRT-PCR of *AXIN2*. **i**, Upregulated APC protein by TMEM9 depletion. *TMEM9* WT and KO cells were analysed by IB. **j**, Increased APC protein by v-ATPase inhibition. HCT116 and HT29 cells were incubated with indicated reagents (HCQ, 25 μ M; BAF, 3 nM; CMA, 0.3 nM) for 6 h. IB analysis and quantification using ImageJ. **k**, APC upregulation by inhibition of lysosomal protein degradation. CRC cells were incubated with cathepsin inhibitors (CA074 and SID26681509) for 12 h. IB and quantification using ImageJ. **l-o**, Loss of TMEM9 depletion downregulated Wnt/ β -catenin signalling by APC KO: HCT116 (**l,m**) and HT29 (**n,o**) cells were analysed for IB and qRT-PCR of *AXIN2*. **p-s**, Increased interaction between APC and β -catenin by *TMEM9* KO: co-IP analysis (**p**); scheme of Duolink assay monitoring APC- β -catenin binding (**q**). Cells were incubated with APC N terminal (mouse) and β -catenin (rabbit) antibody followed by reaction with PLA probes. Dots indicate an interaction between APC and β -catenin (**r**). Protein interaction was quantified (**s**; $n = 10$ independent samples) using manufacturer's software (Sigma). Images are representative of three experiments with similar results. Scale bars, 20 μ m; NS, not significant. Error bars represent mean \pm s.d. from $n = 3$ independent experiments, except for **s**; two-sided unpaired *t*-test.

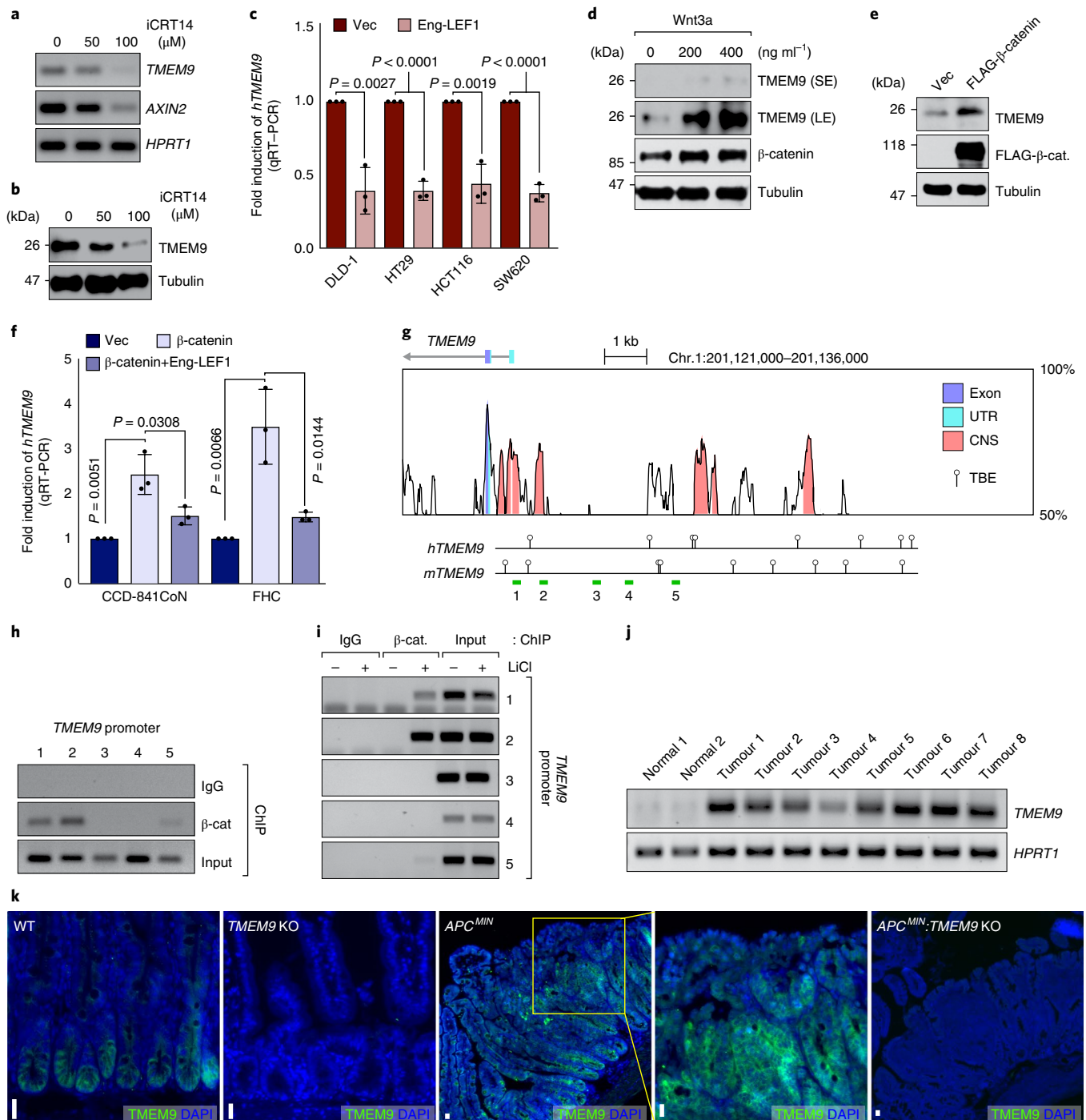


Fig. 5 | Transactivation of *TMEM9* by Wnt/ β -catenin signaling. **a,b, Downregulation of *TMEM9* by β -catenin inhibition. HCT116 cells were treated with iCRT14 for 24 h and analysed by RT-PCR (**a**) and IB (**b**). **c**, Increased *TMEM9* expression by β -catenin in CRC. After inhibition of β -catenin transcription activity by Eng-LEF1, *TMEM9* expression was assessed by qRT-PCR. $n = 3$ independent experiments. Error bars indicate mean \pm s.d.; two-sided unpaired *t*-test. **d**, Upregulation of *TMEM9* by Wnt3a. 293T cells were treated with Wnt3a and analysed by IB. **e**, Increased *TMEM9* by β -catenin. 293T cells were transfected with β -catenin-expressing plasmids and analysed by IB, 48 h after transfection. **f**, Increase of *TMEM9* expression by β -catenin in IECs. IECs were transfected with Vec, β -catenin or Eng-LEF1 plasmids for 48 h. Cells were harvested for qRT-PCR of *TMEM9*. $n = 3$ independent experiments. Error bars indicate mean \pm s.d.; two-sided unpaired *t*-test. **g**, *TMEM9* promoter analysis using VISTA genome browser. UTR, untranslated region; CNS, conserved non-coding sequence; TBE, TCF binding elements (balloons); green bars, PCR amplicons (~1–5). **h**, β -catenin occupancy on the *TMEM9* promoter. HCT116 cells were analysed by ChIP assays. **i**, Conditional recruitment of β -catenin on the *TMEM9* promoter. HeLa cells were treated with LiCl (25 mM, 4 h) and analysed by ChIP assays. **j,k**, Upregulation of *TMEM9* in *APC*^{MIN} intestinal tumours. *TMEM9* expression was examined in two normal small intestinal samples and eight intestinal adenoma samples (~1–8) from *APC*^{MIN} mouse (14 weeks of age) by RT-PCR (**j**) and IHC (**k**). *TMEM9* KO mice served as negative controls (*TMEM9*^{-/-} and *APC*^{MIN};*TMEM9*^{-/-}). Images are representative of three experiments with similar results. Scale bars, 20 μ m.**

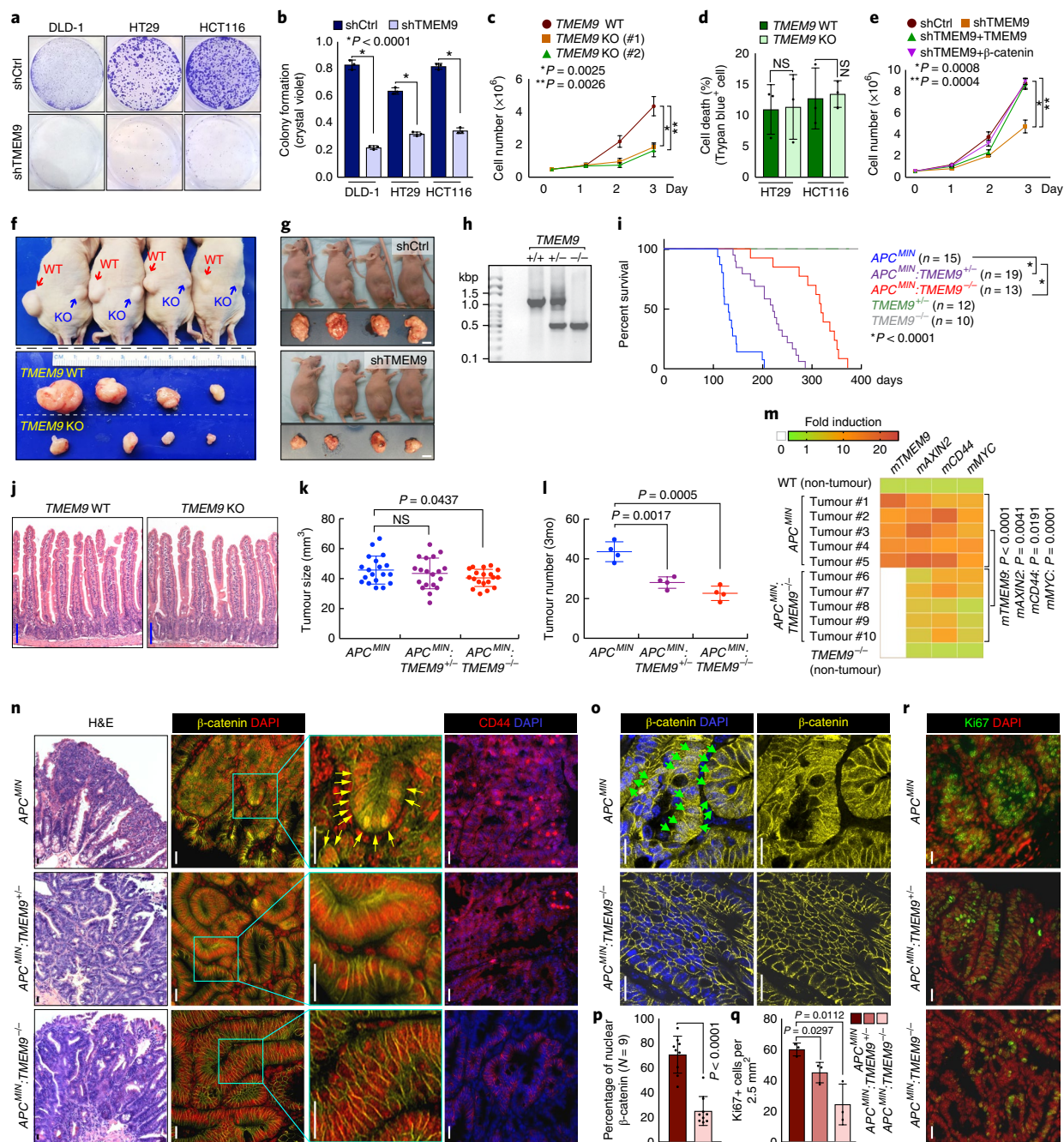


Fig. 6 | Suppression of intestinal tumorigenesis by blockade of TMEM9. **a–c**, Decreased CRC cell proliferation by TMEM9 depletion. Crystal violet staining (**a**) was quantified by absorbance at 590 nm (**b**). HCT116 cell proliferation was analysed by cell counting (**c**). Two different gRNAs (#1 and #2) were used for CRISPR/Cas9 targeting of *TMEM9* alleles. **d**, No effects of *TMEM9* KO on cell death. Trypan blue positive cells were quantified. **e**, Rescue of *TMEM9* depletion-induced cell growth inhibition by *TMEM9* or β -catenin. HCT116 (shCtrl and sh*TMEM9*) cells were stably transduced with *TMEM9* or β -catenin and analysed by cell counting. **f, g**, Reduced CRC cell proliferation by *TMEM9* depletion ex vivo. Each mouse ($n = 4$ biologically independent samples) was subcutaneously injected with 1×10^7 cells into the left (HT29 [Ctrl]) and right flanks (*TMEM9* KO-HT29; **f**). 15 days after transplantation, tumours were harvested. HCT116 (shCtrl and sh*TMEM9*) cells were subcutaneously injected into immunocompromised mice (**g**). Scale bars, 1 cm. Experiments were performed once. **h**, PCR genotyping results of *TMEM9* KO. **i**, Survival curves (Kaplan–Meier analysis) of *APC*^{MIN}, *APC*^{MIN};*TMEM9*^{+/-} and *APC*^{MIN};*TMEM9*^{-/-} mice. **j**, No defects in IEC differentiation by *TMEM9* KO. H&E, haematoxylin & eosin. Scale bars, 100 μ m. **k, l**, Decreased tumour growth by *TMEM9* KO: tumour size (**k**; $n = 19$ independent samples) and tumour number (**l**; $n = 4$ biologically independent samples) were quantified by measuring intestinal adenomas in *APC*^{MIN}, *APC*^{MIN};*TMEM9*^{+/-} and *APC*^{MIN};*TMEM9*^{-/-} mice (3 months of age). Experiments were performed once. **m**, Downregulation of Wnt/ β -catenin target genes by *TMEM9* KO in *APC*^{MIN} adenomas. *APC*^{MIN}- and *APC*^{MIN};*TMEM9* KO-induced tumours and IECs of WT and *TMEM9* KO were collected for qRT-PCR of β -catenin target genes (*AXIN2*, *CD44* and *MYC*) and *TMEM9*. **n**, IHC analysis of intestinal tumours from *APC*^{MIN}, *APC*^{MIN};*TMEM9*^{+/-} and *APC*^{MIN};*TMEM9*^{-/-} mice. Scale bars, 20 μ m. **o, p**, Loss of nuclear β -catenin by *TMEM9* KO in *APC*^{MIN} mice. *APC*^{MIN}- and *APC*^{MIN};*TMEM9* KO-induced tumours were stained with β -catenin antibody (**o**) and quantified ($n = 9$ independent tumours; **p**). Scale bars, 20 μ m. Arrows in **n, o** indicate β -catenin. **q, r**, IHC for Ki67 (**r**) and quantification of Ki67 positive (Ki67+) cells from intestinal tumours (**q**; $n = 3$ independent tumours). Scale bars, 20 μ m. Images and blots are representative of three experiments with similar results (**a–e**, **j** and **m–r**). Error bars indicate mean \pm s.d. Two-sided unpaired *t*-test. NS, not significant.

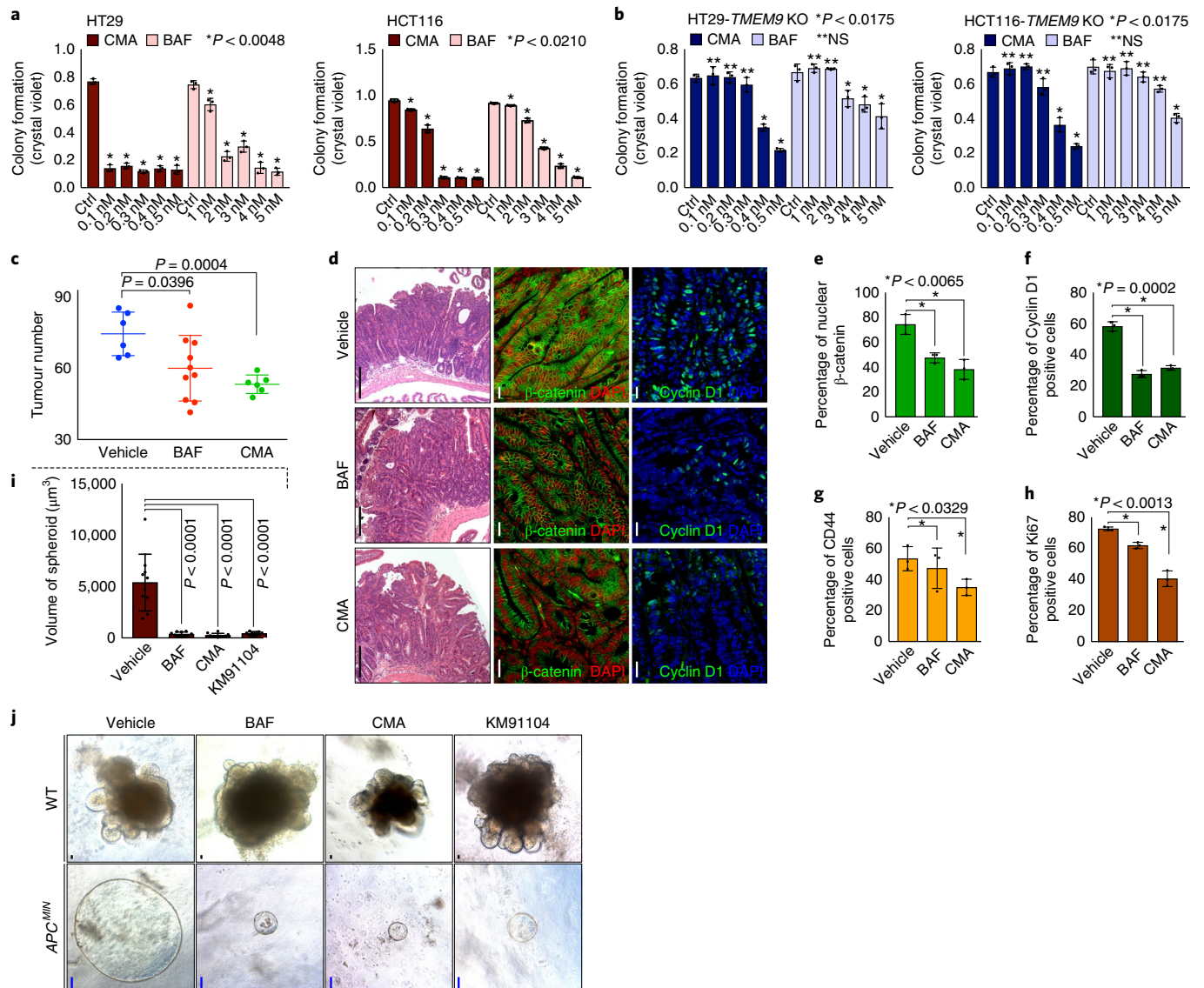


Fig. 7 | Suppression of intestinal tumorigenesis by v-ATPase inhibitors. **a**, Suppressed CRC cell proliferation by v-ATPase inhibitors. CRC cells (1,000 cells) were seeded and treated with v-ATPase inhibitors for 10 days. Cells were then fixed with 4% paraformaldehyde (PFA). After fixation, cells were stained with crystal violet. Cell proliferation was quantified by measuring absorbance at 590 nm. $n = 3$ independent experiments. **b**, Diminished effects of v-ATPase inhibitors on CRC cell growth by *TMEM9* KO. *TMEM9* KO-HT29 and -HCT116 cells (1,000 cells) were incubated with CMA or BAF for 10 days. Quantification of crystal violet staining. $n = 3$ independent experiments. **c**, Decrease of *APC*^{MIN}-induced tumorigenesis by v-ATPase inhibitors. *APC*^{MIN} mice (10 weeks of age) were injected with BAF (3 mg kg⁻¹; $n = 10$ biologically independent samples) or CMA (1 mg kg⁻¹; $n = 6$ biologically independent samples) every 3 days for 6 weeks. Experiments were performed once. **d–h**, Downregulation of Wnt/ β -catenin signalling by v-ATPase inhibitors. After administration of v-ATPase inhibitors every 3 days for 6 weeks, *APC*^{MIN}-induced tumours were stained by H&E for β -catenin, CD44, cyclin D1 and Ki67 (**d**) antibody and quantified (**e–h**). White scale bars, 20 μ m. Black scale bars, 200 μ m. $n = 3$ independent experiments. **i, j**, Growth inhibition of tumour but not crypt organoids by v-ATPase inhibitors. Organoids were derived from the intestinal crypts or tumours of WT C57BL/B6 and *APC*^{MIN} mice (**j**), respectively. At 14 days after incubation with v-ATPase inhibitors, organoid growth was assessed (**i**). Blue scale bars, 20 μ m. $n = 10$ independent samples. Images are representative of three experiments with similar results. Error bars indicate mean \pm s.d.; two-sided unpaired *t*-test.

Inhibition of intestinal tumorigenesis by v-ATPase inhibitors. Having determined that *TMEM9* activates Wnt/ β -catenin signalling via v-ATPase, we next asked whether v-ATPase inhibitors suppress intestinal tumorigenesis. First, we assessed the impacts of v-ATPase inhibitors on CRC cell growth. BAF and CMA significantly inhibited CRC cell proliferation (HT29, HCT116; Fig. 7a). Of note, the impact of v-ATPase inhibitors on CRC cell growth suppression was diminished in *TMEM9* KO CRC cells (Fig. 7b) compared to *TMEM9* WT cells (Fig. 7a). We also examined the effect of v-ATPase inhibitors on CRC using the *APC*^{MIN} mouse model. While the normal intestinal

homeostasis was not affected by v-ATPase inhibitors, *APC*^{MIN} mice treated with BAF or CMA exhibited a decrease in intestinal adenoma number, β -catenin, β -catenin targets and tumour cell proliferation (Fig. 7c–h and Supplementary Fig. 5a,b) compared to vehicle-treated control mice. Similarly, intestinal tumour organoids treated with v-ATPase inhibitors also showed decreased tumour growth, whereas normal crypt organoids exhibited no impairment in growth and expansion (Fig. 7i,j). These results led us to further test the impacts of v-ATPase inhibitors on human CRC, employing patient-derived xenograft (PDX) models. Similar to the mouse results, BAF decreased

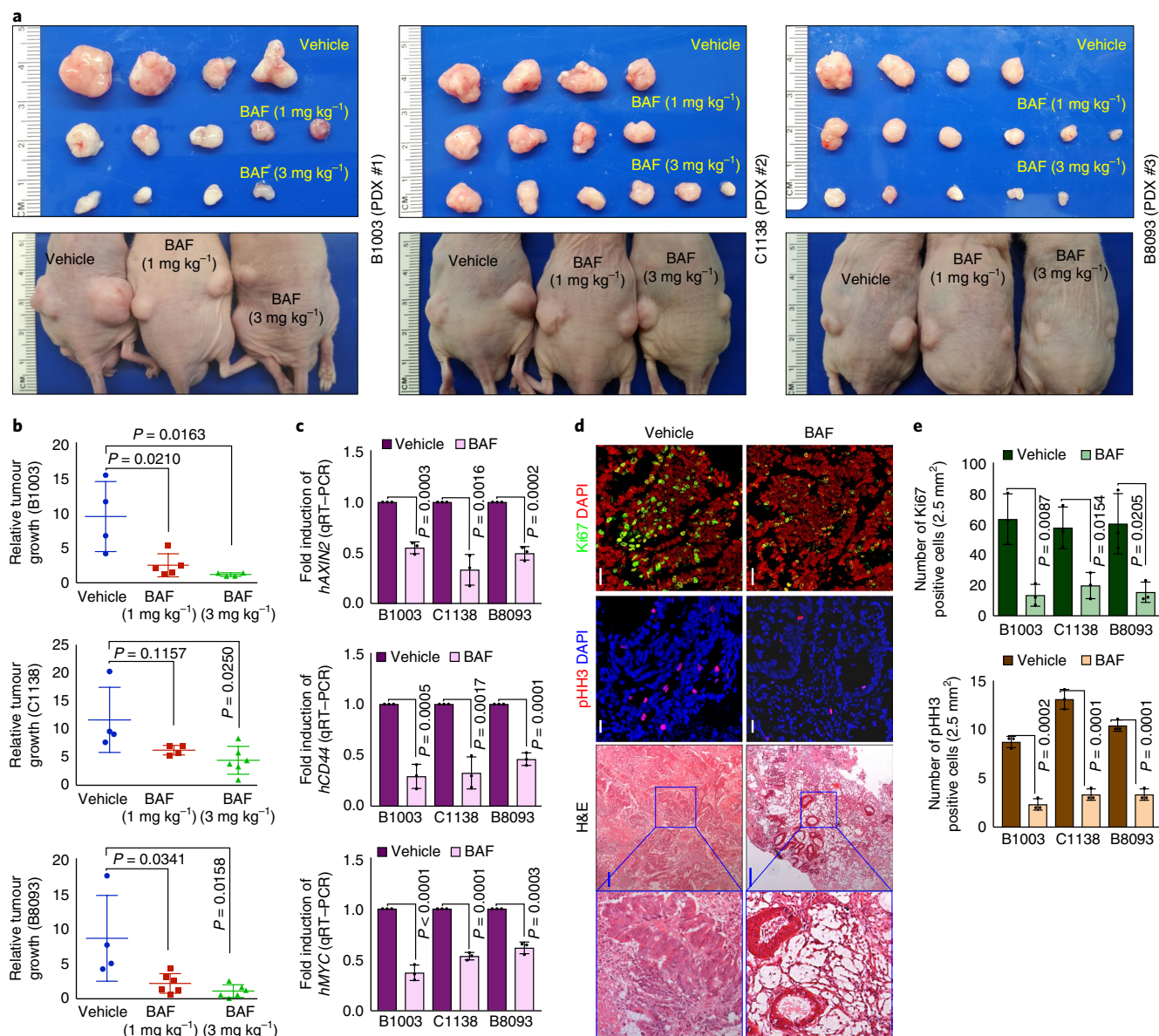


Fig. 8 | Decreased PDX growth by v-ATPase inhibitor. a,b, Suppression of PDX growth by BAF. Immunocompromised mice (BALB/c nude) were subcutaneously transplanted with three PDXs into both right and left flanks. At 7 days after transplantation, mice were injected with vehicle (corn oil; $n = 4$ biologically independent samples) or BAF (1 mg kg^{-1} (B1003; $n = 5$ biologically independent samples; C1138; $n = 4$ biologically independent samples; B8093; $n = 6$ biologically independent samples) or 3 mg kg^{-1} (B1003, $n = 4$ biologically independent samples; C1138, $n = 6$ biologically independent samples; B8093, $n = 5$ biologically independent samples) every 3 days for 15 days (**a**). At 18 days post injection, PDXs were collected for assessment of relative tumour growth (ratio of weight: day18/day0) (**b**). Experiments were performed once. **c**, Downregulation of Wnt/ β -catenin signalling by BAF in the PDX model. qRT-PCR of β -catenin target genes (*hAXIN2*, *hCD44* and *hMYC*). $n = 3$ independent experiments. **d,e**, Decreased cell proliferation by BAF in PDXs. IHC for phosphorylated histone H3 (pHH3, a marker of mitosis) and Ki67 (a marker of proliferative cells): H&E (**d**) and quantification (**e**). White scale bars, $20 \mu\text{m}$. Blue scale bars, $200 \mu\text{m}$. $n = 3$ independent experiments. Images are representative of three experiments with similar results. Error bars indicate mean \pm s.d.; two-sided unpaired *t*-test.

PDX growth (Fig. 8a,b and Supplementary Fig. 6a,b), with reduced β -catenin and target expression (Fig. 8c) and cell proliferation (Ki67, pHH3; Fig. 8d,e and Supplementary Fig. 6c). Additionally, BAF-treated PDXs exhibited an increase of APC and decrease in nuclear β -catenin (Supplementary Fig. 6d,e). These results strongly suggest that the blockade of v-ATPase suppresses intestinal tumorigenesis with reduced Wnt/ β -catenin signalling activity.

Discussion

Several regulatory mechanisms of v-ATPase activity have been proposed. For instance, v-ATPase assembly is reversible^{31,32}

and controlled by E3 ligase³³. TMEM9 is mainly localized in the MVBs and interacts with several components of the proton pump and their accessory proteins, ATP6AP2 and v-ATPase. We found that TMEM9 increases the ATP6AP2–ATP6V0D1 interaction. Given (1) the interaction of TMEM9 with both ATP6AP2 and ATP6V0D1 and (2) the relatively small size of TMEM9 (186 amino acids), it is likely that TMEM9 acts as a molecular adaptor modulating the interaction between ATP6AP2 and ATP6V0D1. Unlike *TMEM9*, other v-ATPase components (*ATP6AP2*, *ATP6V0D1*, *TMEM9B* (a homologous gene of *TMEM9*)) are not upregulated in human CRC (Supplementary Fig. 2f). Thus,

hyperactivation of v-ATPase in CRC might be mainly due to upregulation of *TMEM9*. It has been shown previously that ATP6AP2 binds to LRPs and Fzd to promote Wnt signals¹⁶. However, our mass spectrometry and co-IP results did not detect LRP signalosome components as *TMEM9*-interacting proteins (Fig. 3a,e,f), implying that *TMEM9*-activated Wnt signalling in CRC might be somewhat distinct from ATP6AP2–LRP–Fzd-mediated Wnt signalling activation.

Despite frequent mutations in *APC* (~70%)², accumulating evidence suggests that additional intrinsic and extrinsic factors may further hyperactivate Wnt signalling during tumour initiation and metastasis^{9–11,34}. It has also been shown that mutant *APC* still negatively modulates β -catenin¹⁰. Intriguingly, *TMEM9* activates Wnt/ β -catenin signalling regardless of *APC* mutation status (Fig. 2j and Supplementary Fig. 1h,i). While β -catenin is degraded by β -TrCP-mediated ubiquitination, both MT and WT *APC* are under lysosomal degradation induced by *TMEM9*-v-ATPase-activated vesicular acidification (Fig. 4i–k), suggesting the alternative mechanism of Wnt signalling hyperactivation in CRC. It is also noteworthy that *TMEM9* is transactivated by β -catenin, suggesting that *TMEM9* might function as an amplifier of Wnt signalling in CRC.

TMEM9 KO mice are viable without any discernible phenotype, which might be due to the relatively low expression of *TMEM9* in normal tissues. Given the upregulation of *TMEM9* in CRC cells and its pivotal role in CRC cell proliferation, molecular targeting of the *TMEM9*-v-ATPase axis might provide a potential benefit in CRC treatment, with minimal detrimental effects to normal cells. Indeed, v-ATPase inhibitors displayed strong tumour suppressive effects on CRC suppression in cell lines, organoids, mice and human PDXs, without damage to normal tissues (Figs. 7 and 8).

Together, our results reveal an unexpected positive feedback mechanism of Wnt signalling by *TMEM9*, a regulator of v-ATPase, and propose that the blockade of *TMEM9*-v-ATPase might be a viable option for *TMEM9*-expressing CRC treatment.

Online content

Any methods, additional references, Nature Research reporting summaries, source data, statements of data availability and associated accession codes are available at <https://doi.org/10.1038/s41556-018-0219-8>.

Received: 18 March 2018; Accepted: 21 September 2018;

Published online: 29 October 2018

References

- Clevers, H. & Nusse, R. Wnt/ β -catenin signaling and disease. *Cell* **149**, 1192–1205 (2012).
- Polakis, P. The many ways of Wnt in cancer. *Curr. Opin. Genet. Dev.* **17**, 45–51 (2007).
- Bilic, J. et al. Wnt induces LRP6 signalosomes and promotes Dishevelled-dependent LRP6 phosphorylation. *Science* **316**, 1619–1622 (2007).
- Zeng, X. et al. Initiation of Wnt signaling: control of Wnt coreceptor Lrp6 phosphorylation/activation via Frizzled, Dishevelled and Axin functions. *Development* **135**, 367–375 (2008).
- Cadigan, K. M. & Waterman, M. L. TCF/LEFs and Wnt signaling in the nucleus. *Cold Spring Harb. Perspect. Biol.* **4**, a007906 (2012).
- Taelman, V. F. et al. Wnt signaling requires sequestration of glycogen synthase kinase 3 inside multivesicular endosomes. *Cell* **143**, 1136–1148 (2010).
- Polakis, P. Wnt signaling in cancer. *Cold Spring Harb. Perspect. Biol.* **4**, a008052 (2012).
- Phelps, R. A. et al. A two-step model for colon adenoma initiation and progression caused by *APC* loss. *Cell* **137**, 623–634 (2009).
- Vermeulen, L. et al. Wnt activity defines colon cancer stem cells and is regulated by the microenvironment. *Nat. Cell Biol.* **12**, 468–476 (2010).
- Voloshanenko, O. et al. Wnt secretion is required to maintain high levels of Wnt activity in colon cancer cells. *Nat. Commun.* **4**, 2610 (2013).

- Jung, Y. S., Jun, S., Lee, S. H., Sharma, A. & Park, J. I. Wnt2 complements Wnt/ β -catenin signaling in colorectal cancer. *Oncotarget* **6**, 37257–37268 (2015).
- Niehrs, C. & Boutros, M. Trafficking, acidification, and growth factor signaling. *Sci. Signal.* **3**, pe26 (2010).
- Marshansky, V. & Futai, M. The V-type H⁺-ATPase in vesicular trafficking: targeting, regulation and function. *Curr. Opin. Cell Biol.* **20**, 415–426 (2008).
- Forgac, M. Vacuolar ATPases: rotary proton pumps in physiology and pathophysiology. *Nat. Rev. Mol. Cell Biol.* **8**, 917–929 (2007).
- Mindell, J. A. Lysosomal acidification mechanisms. *Annu. Rev. Physiol.* **74**, 69–86 (2012).
- Cruciat, C. M. et al. Requirement of prorenin receptor and vacuolar H⁺-ATPase-mediated acidification for Wnt signaling. *Science* **327**, 459–463 (2010).
- Buechling, T. et al. Wnt/Frizzled signaling requires dPRR, the *Drosophila* homolog of the prorenin receptor. *Curr. Biol.* **20**, 1263–1268 (2010).
- Hermle, T., Saltukoglu, D., Grunewald, J., Walz, G. & Simons, M. Regulation of Frizzled-dependent planar polarity signaling by a V-ATPase subunit. *Curr. Biol.* **20**, 1269–1276 (2010).
- Wielenga, V. J. et al. Expression of CD44 in *Apc* and *Tcf* mutant mice implies regulation by the WNT pathway. *Am. J. Pathol.* **154**, 515–523 (1999).
- Funayama, N., Fagotto, F., McCrea, P. & Gumbiner, B. M. Embryonic axis induction by the armadillo repeat domain of β -catenin: evidence for intracellular signaling. *J. Cell Biol.* **128**, 959–968 (1995).
- Nishi, T. & Forgac, M. The vacuolar (H⁺)-ATPases—nature's most versatile proton pumps. *Nat. Rev. Mol. Cell Biol.* **3**, 94–103 (2002).
- Kinouchi, K. et al. The (pro)renin receptor/ATP6AP2 is essential for vacuolar H⁺-ATPase assembly in murine cardiomyocytes. *Circ. Res.* **107**, 30–34 (2010).
- O'Brien, C. A. et al. ID1 and ID3 regulate the self-renewal capacity of human colon cancer-initiating cells through p21. *Cancer Cell* **21**, 777–792 (2012).
- Bowman, E. J., Graham, L. A., Stevens, T. H. & Bowman, B. J. The bafilomycin/concanamycin binding site in subunit c of the V-ATPases from *Neurospora crassa* and *Saccharomyces cerevisiae*. *J. Biol. Chem.* **279**, 33131–33138 (2004).
- Gross, J. C., Chaudhary, V., Bartscherer, K. & Boutros, M. Active Wnt proteins are secreted on exosomes. *Nat. Cell Biol.* **14**, 1036–1045 (2012).
- Urbanelli, L. et al. Signaling pathways in exosomes biogenesis, secretion and fate. *Genes* **4**, 152–170 (2013).
- Yang, J. et al. Adenomatous polyposis coli (APC) differentially regulates β -catenin phosphorylation and ubiquitination in colon cancer cells. *J. Biol. Chem.* **281**, 17751–17757 (2006).
- Mauvezin, C., Nagy, P., Juhasz, G. & Neufeld, T. P. Autophagosome-lysosome fusion is independent of V-ATPase-mediated acidification. *Nat. Commun.* **6**, 7007 (2015).
- Montross, W. T., Ji, H. & McCrea, P. D. A β -catenin/engrailed chimera selectively suppresses Wnt signaling. *J. Cell Sci.* **113**, 1759–1770 (2000).
- Su, L. K. et al. Multiple intestinal neoplasia caused by a mutation in the murine homolog of the APC gene. *Science* **256**, 668–670 (1992).
- Kane, P. M. Disassembly and reassembly of the yeast vacuolar H⁺-ATPase in vivo. *J. Biol. Chem.* **270**, 17025–17032 (1995).
- Graf, R., Harvey, W. R. & Wiczorek, H. Purification and properties of a cytosolic V1-ATPase. *J. Biol. Chem.* **271**, 20908–20913 (1996).
- Smardon, A. M., Tarsio, M. & Kane, P. M. The RAVE complex is essential for stable assembly of the yeast V-ATPase. *J. Biol. Chem.* **277**, 13831–13839 (2002).
- Najdi, R., Holcombe, R. F. & Waterman, M. L. Wnt signaling and colon carcinogenesis: beyond APC. *J. Carcinog.* **10**, 5 (2011).

Acknowledgements

The authors thank X. Wang and A. Sharma for technical assistance. This work was supported by the University of Texas McGovern Medical School (startup funding to R.K.M.), the Cancer Prevention Research Institute of Texas (RP140563 to J.-I.P.), the National Institutes of Health (R01 CA193297-01 to J.-I.P.; 5R01 GM107079 to P.D.M.; K01DK092320 to R.K.M.; R01 GM126048 to W.W.), the Department of Defense Peer Reviewed Cancer Research Program (CA140572 to J.-I.P.), a Duncan Family Institute for Cancer Prevention and Risk Assessment Grant (IRG-08-061-01 to J.-I.P.), a Center for Stem Cell and Developmental Biology Transformative Grant (MD Anderson Cancer Center to J.-I.P.), an Institutional Research Grant (MD Anderson Cancer Center to J.-I.P.), a New Faculty Award (MD Anderson Cancer Center Support Grant to J.-I.P.), a Metastasis Research Center Grant (MD Anderson to J.-I.P.) and a Uterine SPORE Career Enhancement Program (MD Anderson to J.-I.P.). The core facility (DNA sequencing and Genetically Engineered Mouse Facility) was supported by an MD Anderson Cancer Center Support Grant (CA016672).

Author contributions

Y.-S.J., S.J., H.Y.J., and J.-I.P. conceived and designed experiments. Y.-S.J., S.J., M.J.K., S.H.L., H.N.S., E.M.L., H.-Y.J., S.L., J.Z., J.-I.Y., H.J., W.W., R.K.M., and J.-I.P. performed experiments. J.Y.W. and S.K. provided samples. Y.-S.J., W.W., S.L., H.-Y.J., R.K.M., J.C., P.D.M. and J.-I.P. analysed data. Y.-S.J. and J.-I.P. wrote the manuscript.

Competing interest

The authors declare no competing interests.

Additional information

Supplementary information is available for this paper at <https://doi.org/10.1038/s41556-018-0219-8>.

Reprints and permissions information is available at www.nature.com/reprints.

Correspondence and requests for materials should be addressed to J.-I.P.

Publisher's note: Springer Nature remains neutral with regard to jurisdictional claims in published maps and institutional affiliations.

© The Author(s), under exclusive licence to Springer Nature Limited 2018

Methods

Tandem affinity purification and mass spectrometry. Cells were grown in twenty 10 cm dishes until reaching 80% confluence, then harvested in a 250 ml centrifuge bottle (Corning). After centrifuging at 300 g for 5 min at 4 °C, cell pellets were suspended in 30 ml PBS. After centrifuging once more under the same conditions, cells were incubated with ~10–15 ml ice-cold NETN buffer (20 mM Tris-HCl pH 8.0, 100 mM NaCl, 0.5 mM EDTA and 0.5% (v/v) Nonidet P-40; freshly added with the proteinase and phosphatase inhibitors) on a shaker at 4 °C for 20 min. Lysates were subjected to centrifugation at 4 °C and 13,148 g for 15 min. Transferred supernatants were incubated with streptavidin-conjugated beads (Amersham) for 1 h at 4 °C. After washing three times with NETN buffer, the beads were transferred to a new tube, and interacted proteins were eluted with 1.5 ml NETN buffer with 2 mg ml⁻¹ biotin (Sigma) for about 90 min at 4 °C. The eluted proteins were transferred and incubated with S protein beads (Novagen) for 1 h. The beads were subjected to SDS-PAGE after three washing steps. Protein bands were excised and subjected to mass spectrometry analysis.

After cutting excised gel bands into ~1 mm³ pieces, in-gel trypsin digestion was performed. Dried samples were reconstituted in 5 µl of HPLC solvent A (2.5% acetonitrile, 0.1% formic acid). By packing 5 µm C18 spherical silica beads into a fused-silica capillary (100 µm inner diameter × ~20 cm length) with a flame-drawn tip, a nanoscale reverse-phase HPLC capillary column was created. After equilibrating the column, each sample was loaded using a Famos autosampler (LC Packings) onto the column, and peptides were eluted with increasing concentrations of solvent B (97.5% acetonitrile, 0.1% formic acid). Eluted peptides were subjected to electrospray ionization and then entered into an LTQ Velos ion-trap mass spectrometer (ThermoFisher). After detecting, isolating and fragmenting peptides to produce a tandem mass spectrum of specific fragment ions for each peptide, peptide sequences were determined by matching protein databases (the human IPI database version 3.6) with the acquired fragmentation pattern using the software program SEQUEST (version 28) (ThermoFisher). The specificity of the enzyme was set to partially tryptic with two missed cleavages. Carboxyamidomethyl (cysteines, fixed) and oxidation (methionine, variable) were included in the modification. Mass tolerance was set to 2.0 for precursor ions and 1.0 for fragment ions. To contain less than 1% false discovery rate at the peptide level, spectral matches were filtered based on the target-decoy method³⁵. Finally, only tryptic matches were reported and spectral matches were manually examined. Matched peptides to multiple proteins were assigned so that only the most logical protein was included (Occam's razor).

Oncomine database analysis. Using Oncomine (www.oncomine.org), cDNA microarray data sets of colon adenocarcinoma and normal tissue samples were analysed ($P < 0.0001$; fold change > 2; 10% top ranked).

Constructs. All gene expression plasmids were constructed from cDNA library or open reading frame sources using PCR, and cloned into FLAG-pcDNA, HA-pcDNA, HA-pWZL or FLAG-pMGIB mammalian expression plasmids. Mutant constructs were generated by site-directed mutagenesis using PCR.

Establishment of TMEM9 KO mouse animal model. ESCs targeted with KO-first condition ready targeting vector (#28436; MGI: 1913491; *Tmem9*^{tm1a(EUCOMM)Wts}) were purchased from EUCOMM. Targeted ESCs were cultured for clonal selection and karyotyping. Two clones were injected into the blastocysts to generate chimaeric mice. The germline transmission was confirmed by genotyping, and two founder strains were obtained. Breeding with FLP_{er} deleter removed the PGK_{Neo} selection cassette to generate *TMEM9*^{flxed/+} strain. Then, a *TMEM9*^{flxed/+} strain was bred with CMV-Cre, resulting in *TMEM9*^{-/-} strain. For genotyping, two primers (F2: 5'-GCATAACGATACCACGATATCAAC-3'; R2: 5'-GGAGTGTACTCTTCTCCTAGCATC-3') were used. Wild-type or KO *TMEM9* allele was amplified as 1,243 bp and 416 bp, respectively. All animal procedures were performed based on the guidelines of the Association for the Assessment and Accreditation of Laboratory Animal Care (AAALAC), and institutional (MD Anderson Cancer Center) approved protocols (IACUC00001141; University of Texas MD Anderson Cancer Center Institutional Animal Care and Use Committee). The study is compliant with all relevant ethical regulations regarding animal research.

TMEM9 somatic cell targeting. The KO cells were established using the clustered regularly interspaced short palindromic repeat (CRISPR) using a lentiviral vector (Addgene). The lentiviral plasmid contains two expression cassettes, hSpCas9 and the chimaeric guide RNA (gRNA) where oligos were cloned, based on the protospacer adjacent motif (PAM) on the target site. The lentiCRISPR plasmids were transfected into HEK293T cells along with pCMV-ΔR8.2 dVPR and pCMV-VSVG plasmids for lentiviral packaging. CRU cell lines were then transduced with lentiviruses and selected in puromycin for 72 h. After selection, three clonally selected cell lines were used for analysis. KO was confirmed by IB and genomic DNA sequencing. *TMEM9* gRNA sequences: #1: 5'-GCTGTGCGAGTGCAGGTACG-3'; #2: 5'-CTGATCCGAAAGCCGGATGC-3'.

Mammalian cell culture. Cell lines were purchased from American Type Culture Collection and maintained in Dulbecco's modified Eagle medium (containing 10% fetal bovine serum and 1% penicillin-streptomycin). Mycoplasma screening was performed using a MycoAlert Mycoplasma Detection Kit (Lonza). Lentiviral plasmids encoding shRNAs were purchased from Open Biosystems. To establish cell lines stably expressing shRNAs or genes, each cell line was transduced with lenti- or retroviruses, and selected by puromycin (1–2 µg ml⁻¹) for two days. The following reagents were also used: Wnt3A (R&D), iCRT14 (Santa Cruz)³⁶, bafilomycin (Wako) and concanamycin (Sigma).

Axis duplication assays. *X. laevis* embryos were microinjected with in vitro transcribed mRNAs into ventro-vegetal regions at the four-cell-stage of *X. laevis* embryos³⁷. For gene expression, mRNAs were injected at the one-cell stage and analysed by IB.

Reporter assays. The reporter plasmids, pMegaTOPFLASH and pMegaFOPFLASH³⁸, were transiently transfected with pSV40-Renilla plasmid (internal control) and analysed using a dual luciferase assay system (Promega).

Immunofluorescence staining and IHC. Using Fugene6, cells were transiently transfected with plasmids. Cells grown on glass coverslips were washed and fixed in 4% PFA for 10 min at 4 °C. After blocking with 5% goat serum in PBS, proper antibodies were treated for immunostaining cells. For xenograft staining, samples were collected and fixed in 10% formalin. After processing for paraffin embedding, sectioned samples were immunostained following standard protocols. Cellular co-localization quantification was analysed using ImageJ with the Organelle Based Colocalisation (OBCOL) plugin. Detailed information regarding the antibodies is provided in Supplementary Table 3.

Gene expression analysis. RNAs were extracted by TRIzol and converted to cDNAs using SuperScript II (Invitrogen) with random hexamer. For gene expression analysis, semiquantitative RT-PCR or qRT-PCR was performed. qRT-PCR results were quantified by comparative 2^{-ΔΔCt} methods. For internal controls, *18S* or *HPRT1* was used. Primer sequences are provided in Supplementary Table 2.

Xenograft assays. Mice (BALB/c nude) were subcutaneously injected with 2 × 10⁶ HCT116 cells or 1 × 10⁷ HT29 cells. After 6 and 3 weeks for adaptation, respectively, tumours were quantified, and IHC was performed.

ATPase activity assays. ATPase activity of co-IPs of transfected HeLa cells was measured using PiColorlock Gold Kit (Novus Biologicals). Briefly, co-IPs were incubated with PiColorlock substrate and assessed for generated P_i under a wavelength of 595 nm. Before reaction, endogenous P_i was removed using PiBind resin (Novus Biologicals).

Immunoblotting and immunoprecipitation. Whole-cell lysates of mammalian cells were prepared using NP-40 lysis buffer (0.5% NP-40, 1.5 mM MgCl₂, 25 mM HEPES, 150 mM KCl, 10% glycerol, 1 mM phenylmethylsulfonyl fluoride, 12.7 mM benzamidine HCl, 0.2 mM aprotinin, 0.5 mM leupeptin and 0.1 mM pepstatin A) for 20 min at 4 °C followed by centrifugation (13,148 g for 10 min). Supernatants were denatured in 5× SDS sample buffer (200 mM Tris-HCl pH 6.8, 40% glycerol, 8% SDS, 200 mM dithiothreitol and 0.08% bromophenol blue) at 95 °C for 5 min followed by SDS-PAGE. For immunoblot blocking and antibody incubation, 0.1% non-fat dry milk in Tris-buffered saline and Tween-20 (25 mM Tris-HCl pH 8.0, 125 mM NaCl and 0.5% Tween-20) was used. SuperSignal West Pico (Thermo; 34087) and Femto (Thermo; 34095) reagents were used to detect horseradish peroxidase-conjugated secondary antibodies. For immunoprecipitation, cell lysates were incubated with 20 µl of magnetic beads (Sigma; M8823) for 2 h. Immunoprecipitates were then washed with cell lysis buffer three times, eluted using an SDS sample buffer, and analysed using immunoblotting. Detailed information about antibodies is provided in Supplementary Table 3.

Chromatin immunoprecipitation assay. Cells were crosslinked with 1% formaldehyde for 15 min at room temperature, and quenched by glycine (0.125 M). After washing with cold PBS, tissues were incubated with lysis buffer (0.5% NP-40, 25 mM HEPES, 150 mM KCl, 1.5 mM MgCl₂, 10% glycerol and KOH pH 7.5) containing protease inhibitor for 15 min on ice. Cell lysates were centrifuged (1,677 g for 5 min), and supernatants were discarded. Cell pellets were subjected to sonication with ChIP-radioimmunoprecipitation assay (RIPA) lysis buffer (50 mM Tris, pH 8.0; 150 mM NaCl; 0.1% SDS, 0.5% deoxycholate, 1% NP-40 and 1 mM EDTA; 10 times, 30 s on/30 s off), using Bioruptor Plus sonication device (Diagnode). After centrifugation (11,688 g for 30 min), the supernatant was immunoprecipitated with antibody overnight at 4 °C and was pulled down using Dynabeads Magnetic Beads (Thermo). Immunoprecipitates were also washed serially with ChIP-RIPA lysis buffer, high salt (50 mM Tris, pH 8.0; 500 mM NaCl; 0.1% SDS, 0.5% deoxycholate, 1% NP-40 and 1 mM EDTA), LiCl wash buffer (50 mM Tris, pH 8.0; 1 mM EDTA, 250 mM LiCl; 1% NP-40 and 0.5% deoxycholate) and Tris-EDTA buffer. Finally, immunoprecipitate crosslinking

was reversed by incubation at 65°C overnight and treated with RNase A and proteinase K to extract DNA. The ChIP PCR primer sequences are provided in Supplementary Table 2.

Duolink assays. For visualization of protein interaction in situ, cells were seeded onto the cover glass. After fixation with 4% formalin for 5 min, cells were permeabilized with 0.01% Triton-x100 for Duolink assays, according to the manufacturer's recommended protocol (Sigma; DUO92101): blocking, primary antibody reaction, (+) and (-) probe reaction, ligation, polymerization and amplification.

Organoids culture. In line with previous literature³⁹, we isolated crypt and maintained crypt with organoid culture Advanced DMEM/F12 (Invitrogen) medium containing growth factors (50 ng ml⁻¹ epidermal growth factor (Peprotech), 500 ng ml⁻¹ R-spondin (R&D), 100 ng ml⁻¹ Noggin (Peprotech) and 10 µM Y-27632 (Sigma)). After crypt/spheroid organoid formation for 5 days, organoids were collected and fixed in 10% formalin for IHC.

Vesicle acidification analysis. For visualization of vesicle acidification, cells were seeded onto a cover glass, and, according to the manufacturer's recommended protocol (Invitrogen; L7528), cells were stained with LysoTracker.

PDX transplantation. Patients-derived tumour tissues were subcutaneously transplanted into Nude (BALB/c nude) mice. At 7 days after transplantation, mice were injected with vehicle (corn oil) or Baf A1 (1 mg kg⁻¹ or 3 mg kg⁻¹) every 3 days for 15 days. At 18 days post injection, PDXs were collected for tumour weight quantification, IHC and qRT-PCR. All animal procedures were performed based on the guidelines of the AAALAC and institutionally (MD Anderson Cancer Center) approved protocols (IACUC Study, #00001141; IRB, #LAB10-0982). The study is compliant with all relevant ethical regulations regarding animal research. All study participants provided IRB-approved informed consent for their medical records and tissue samples to be used in this study. The study is compliant with all relevant ethical regulations regarding research involving human participants.

TMA analysis. After pathological analysis (grade and percentage of TMEM9, β-catenin and CD44 expression in TMA (adjacent colon versus CRC), H score was calculated by the following formula: [1 × (% cells 1+) + 2 × (% cells 2+) + 3 × (% cells 3+)].

Statistics and reproducibility. Student's *t*-test was used for comparisons of two groups (*n* ≥ 3). *P* values less than 0.05 were considered significant. Error bars indicate s.d. except the experiments shown in Supplementary Fig. 4e,

which indicate s.e.m. All experiments were performed three or more times with similar results, independently under identical or similar conditions, except the experiments shown in Figs. 1e–g and 3k, which were performed twice, and the experiments in Figs. 2r, 3a, 6f,g,k,l, 8a,b and Supplementary Fig. 6b, which were performed once.

Primer information. See Supplementary Table 2 for a complete list of primers.

Antibody information. See Supplementary Table 3 for a complete list of antibodies.

Reporting Summary. Further information on experimental design is available in the Nature Research Reporting Summary linked to this article.

Data availability

Microarray data that support the findings of this study have been deposited in the Gene Expression Omnibus (GEO) under accession code GDS2947. The TMEM9 expression data in CRC cells were derived from the cBioportal using the TCGA Research Network (<http://cancergenome.nih.gov/>) and Genetech data sets. The data set derived from this resource that supports the findings of this study is available in OncoPrint (<https://www.oncoprint.org/resource>). TMEM9 expression data were also derived from cBioportal (<http://www.cbioportal.org/>) and the COSMIC database (Catalogue of Somatic Mutations in Cancer) (<https://cancer.sanger.ac.uk/cosmic>). Source data for Figs. 1–8 and Supplementary Figs. 1–4 are provided as Supplementary Table 4. All other data supporting the findings of this study are available from the corresponding author on reasonable request.

References

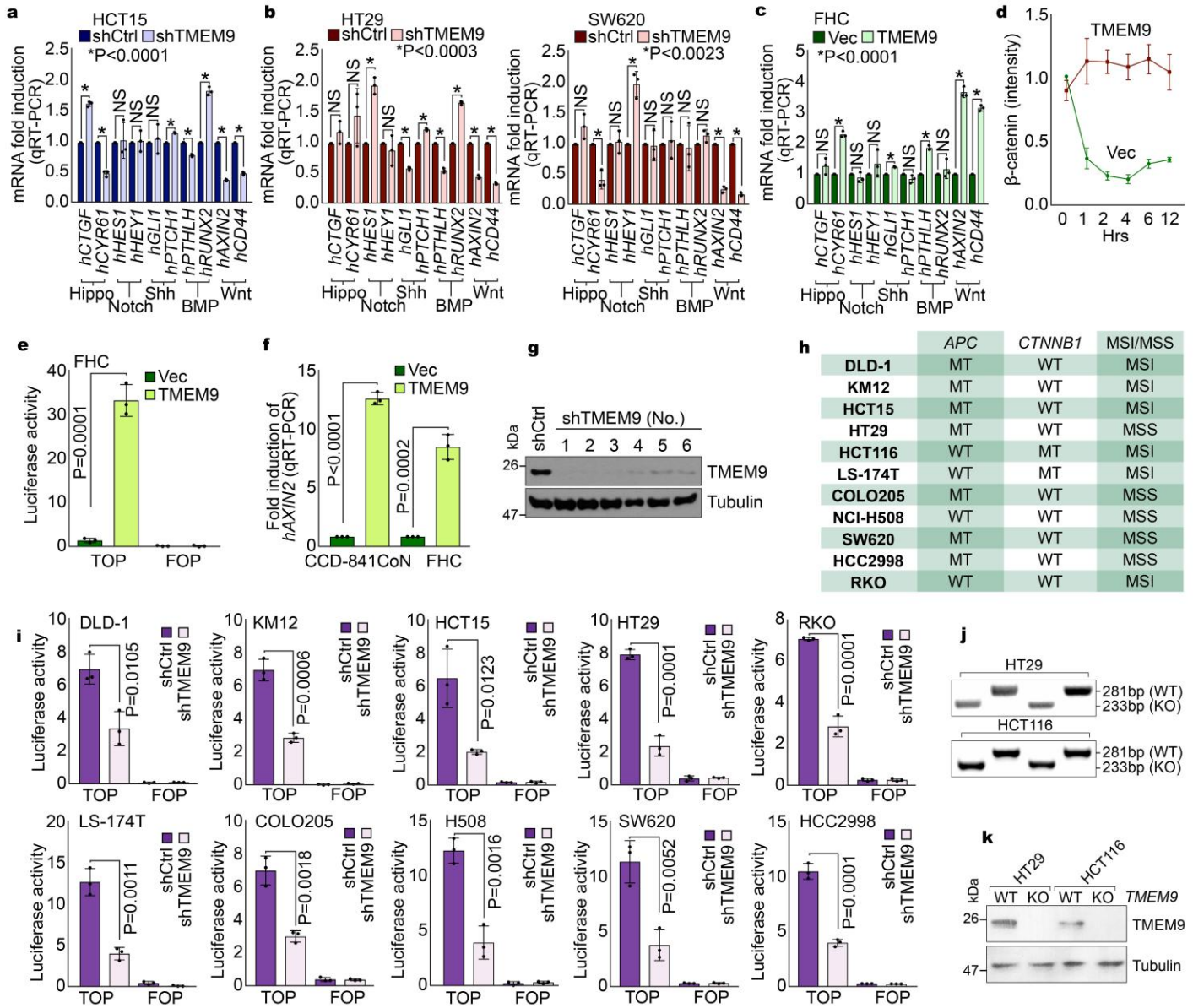
- Elias, J. E. & Gygi, S. P. Target-decoy search strategy for increased confidence in large-scale protein identifications by mass spectrometry. *Nat. Methods* **4**, 207–214 (2007).
- Gonsalves, F. C. et al. An RNAi-based chemical genetic screen identifies three small-molecule inhibitors of the Wnt/wingless signaling pathway. *Proc. Natl Acad. Sci. USA* **108**, 5954–5963 (2011).
- Kuhl, M. & Pandur, P. Dorsal axis duplication as a functional readout for Wnt activity. *Methods Mol. Biol.* **469**, 467–476 (2008).
- Park, J. I. et al. Telomerase modulates Wnt signalling by association with target gene chromatin. *Nature* **460**, 66–72 (2009).
- Sato, T. et al. Single Lgr5 stem cells build crypt-villus structures in vitro without a mesenchymal niche. *Nature* **459**, 262–265 (2009).

In the format provided by the authors and unedited.

TMEM9 promotes intestinal tumorigenesis through vacuolar-ATPase-activated Wnt/ β -catenin signalling

Youn-Sang Jung ^{1,8}, Sohee Jun^{1,8}, Moon Jong Kim¹, Sung Ho Lee¹, Han Na Suh¹, Esther M. Lien¹, Hae-Yun Jung¹, Sunhye Lee¹, Jie Zhang¹, Jung-In Yang¹, Hong Ji², Ji Yuan Wu³, Wenqi Wang ⁴, Rachel K. Miller^{2,5,6,7}, Junjie Chen^{1,6,7}, Pierre D. McCreary^{2,6,7}, Scott Kopetz³ and Jae-Il Park ^{1,6,7*}

¹Department of Experimental Radiation Oncology, The University of Texas MD Anderson Cancer Center, Houston, TX, USA. ²Department of Genetics, The University of Texas MD Anderson Cancer Center, Houston, TX, USA. ³Department of Gastrointestinal Medical Oncology, The University of Texas MD Anderson Cancer Center, Houston, TX, USA. ⁴Department of Developmental and Cell Biology, University of California, Irvine, Irvine, CA, USA. ⁵Department of Pediatrics, The University of Texas McGovern Medical School, Houston, TX, USA. ⁶Graduate School of Biomedical Sciences at Houston, The University of Texas Health Science Center and MD Anderson Cancer Center, Houston, TX, USA. ⁷Program in Genes and Epigenetics, The University of Texas MD Anderson Cancer Center, Houston, TX, USA. ⁸These authors contributed equally: Youn-Sang Jung and Sohee Jun. *e-mail: jaeil@mdanderson.org

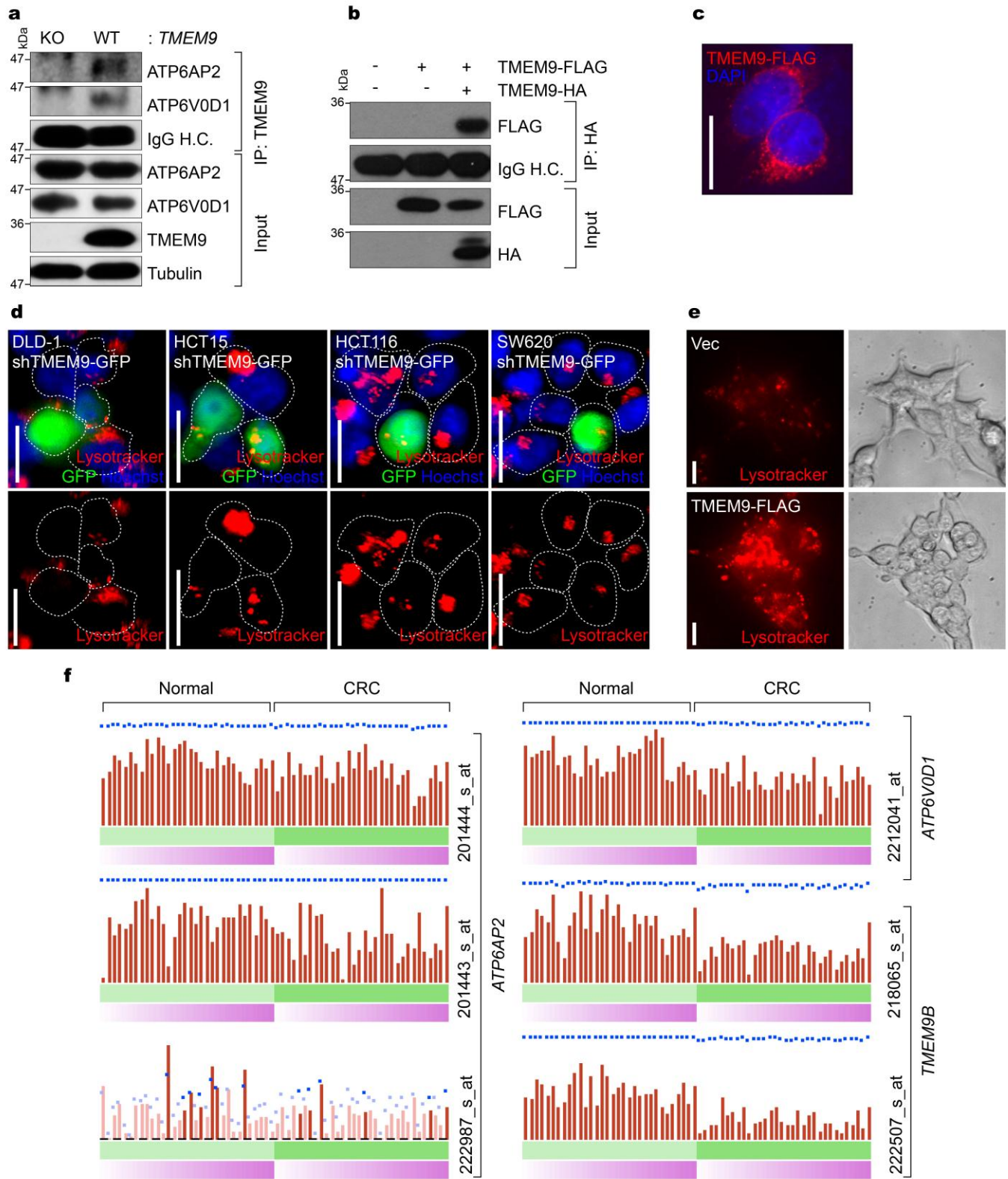


Supplementary Figure 1

Activation of Wnt/β-catenin signaling by TMEM9

a-c, Screening of cell signalings affected by TMEM9. qRT-PCR of CRC cells (MSI [a] vs. MSS [b]) and IECs (c). **d**, Activation of β-catenin by TMEM9 ectopic expression. HeLa cells (Ctrl vs. TMEM9-FLAG) were analyzed for β-catenin protein half-life using cycloheximide (CHX; 100μg/ml), and quantified by ImageJ. **e and f**, Upregulation of β-catenin transcriptional activity by TMEM9 in IECs. 48hr after overexpression of TMEM9, cells were analyzed by luciferase activity (e) and AXIN2 qRT-PCR (f). **g-i**, Decreased β-catenin transcription activity by shTMEM9. Depletion of endogenous TMEM9 using multiple shRNAs (#1-6) in HCT116. HCT116 cells were stably transduced with lentiviruses encoding six different shRNAs and analyzed by IB (g). Eleven CRC cells were analyzed for determination of the effect of TMEM9 on Wnt/β-catenin signaling hyperactivation. (h). TOP/FOP-FLASH luciferase activity (i). **j and k**, Establishment of *TMEM9* KO CRC cells. Exon2 of *TMEM9* was deleted using CRISPR/Cas9 gene targeting. PCR genotyping of *TMEM9* displayed deletion of *TMEM9* (WT: 281bp; KO: 233bp; j). TMEM9 protein was not expressed in *TMEM9* KO CRC cells (k).

NS: Not significant; Experiments were performed three times with similar results; Error bars: mean ± S.D.; Two-sided unpaired t-test.

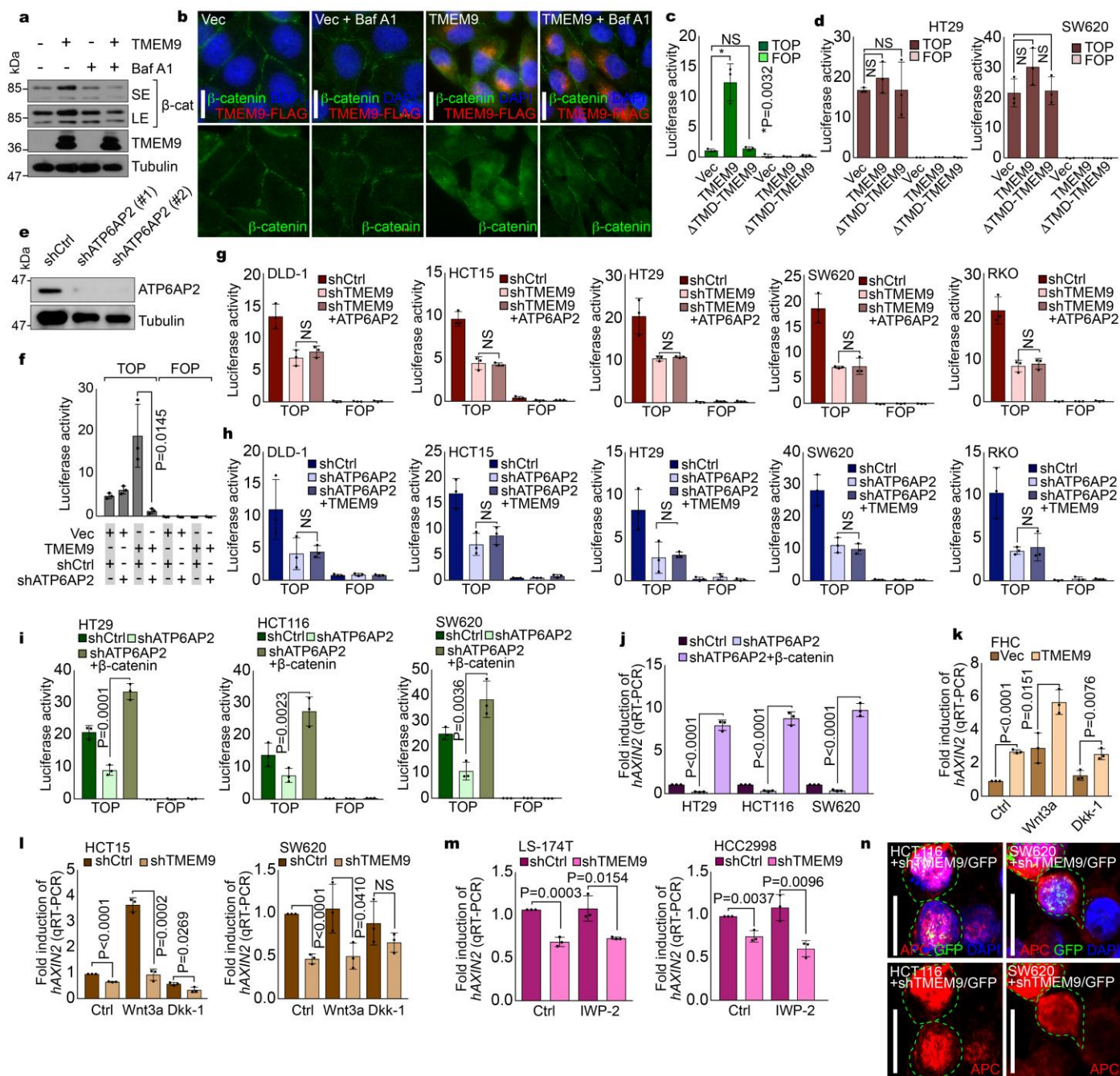


Supplementary Figure 2

TMEM9 facilitates assembly of v-ATPase

a, The endogenous interaction of TMEM9 with ATP6AP2 and APT6V0D1. Co-IP of HCT116 cells (*TMEM9* WT vs. KO). IgG H.C.: immunoglobulin heavy chain. Experiments were performed three times with similar results. **b**, Oligomerization of TMEM9. 293T cells were transfected with each plasmid (TMEM9-FLAG or TMEM9-HA) and were analyzed by co-IP assays. Experiments were performed three times with similar results. **c**, Subcellular localization of ectopically expressed TMEM9. HeLa cells were transfected with TMEM9-FLAG plasmid. After fixation cells were stained with FLAG antibody. **d and e**, Decreased MVB acidification by TMEM9 depletion. CRC (**d**) and 293T (**e**) cells were transfected with shTMEM9-GFP or TMEM9-FLAG plasmid for 24hr, respectively. After transfection cells were stained with LysoTracker for monitoring of MVB acidification. **f**, Expression of *TMEM9B*, *ATP6AP2*, and *ATP6V0D1*. GEO datasets (GDS2947) from NCBI were analyzed for each gene expression in normal intestine and the matched CRC samples (32 patient samples). Of note, *TMEM9B* and other v-ATPase subunits are not upregulated in CRC.

Representative images of three independent experiments with similar results;; Scale bars=20µm.



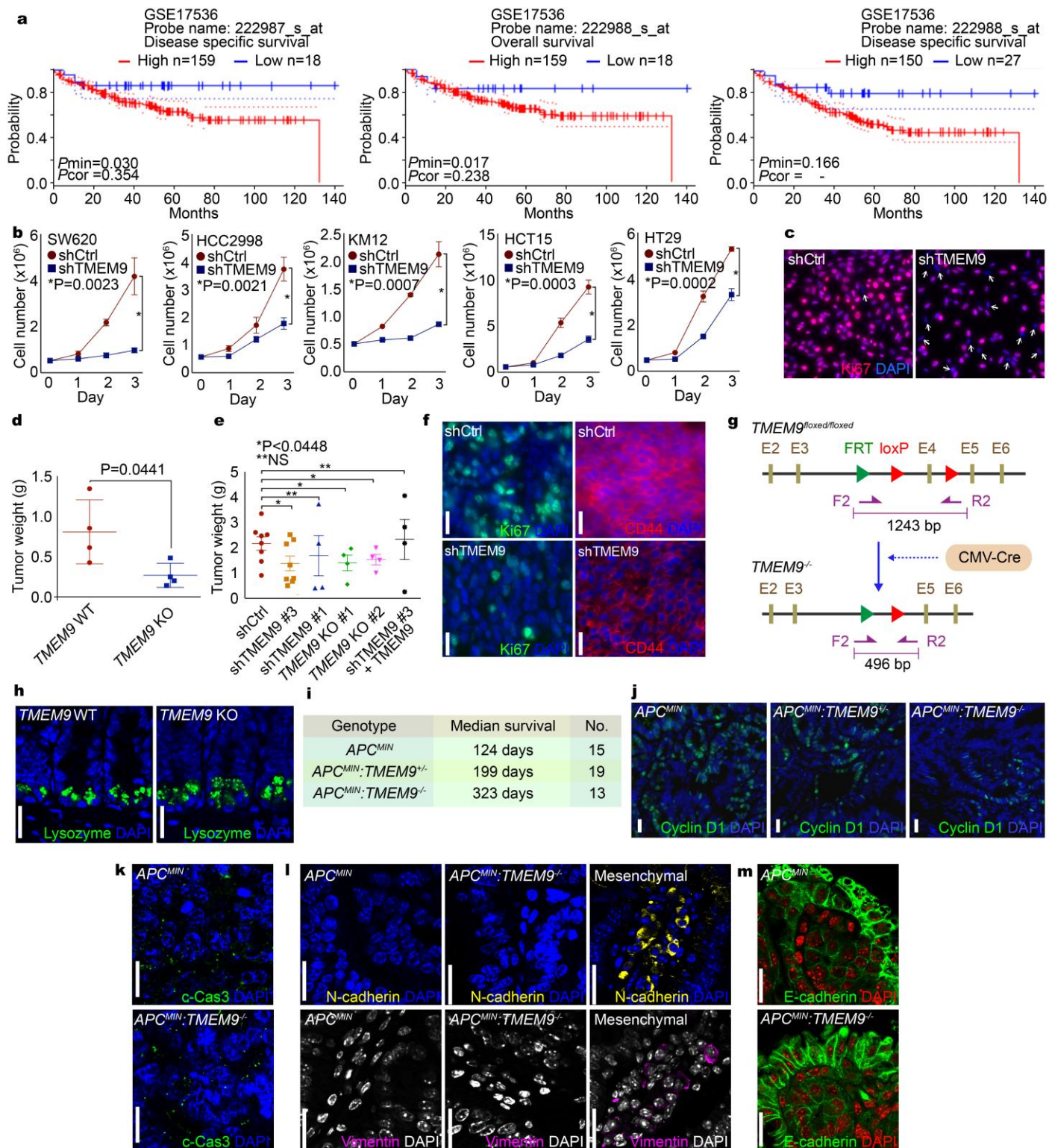
Supplementary Figure 3

TMEM9 activates Wnt/β-catenin signaling via v-ATPase-mediated lysosomal degradation of APC

a-d, Activation of Wnt/β-catenin signaling by TMEM9-activated v-ATPase. TMEM9-induced β-catenin stabilization via v-ATPase (**a** and **b**). HeLa cells stably expressing control Vec or TMEM9-FLAG were treated with BAF (10nM, 24hr) and analyzed by IB (**a**) and IF staining (**b**). The requirement of TMEM9-TMD for TMEM9-induced β-catenin reporter activation (**c** and **d**). 293T (**c**) and CRC (HT29 and SW620; **d**) cells were transfected with WT or TMD deleted MT (ΔTMD) TMEM9 plasmids and analyzed by luciferase assays. The firefly luciferase plasmids and SV40-renilla luciferase expression plasmids (internal control for the transfection efficiency) were transfected into CRC cells for measurement of luciferase activity. 24hr after transfection, cell lysates were assessed by using Dual luciferase assay kit (Promega). Then, the firefly luciferase activity was normalized by the renilla luciferase activity for quantification. **e** and **f**, ATP6AP2 depletion inhibits TMEM9-activated β-catenin reporter. 293T cells stably expressing shRNAs (shCtrl or shATP6AP2 [#1 and #2; two different shRNAs]) were confirmed by IB (**e**), and transfected with the β-catenin reporter and TMEM9 expression plasmids for luciferase assays (**f**). **g** and **h**, No effect of ATP6AP2 and TMEM9 on β-catenin reporter activity in TMEM9 or ATP6AP2

depleted CRC cells. shCtrl, shTMEM9 (**g**), or shATP6AP2 (**h**) plasmids were co-transfected with ATP6AP2 (**g**) or TMEM9 (**h**) plasmids, respectively. **i and j**, Rescue of β -catenin transcription activity by β -catenin overexpression in ATP6AP2 depleted CRC cells. 24hr after transfection, cells were collected for assessment of luciferase activity (**i**) and *AXIN2* expression (**j**). **k and l**, Activation of β -catenin transcription activity by TMEM9 independently of Wnt agonist or antagonist. IECs (**k**) and CRC cells (**l**) were treated with Wnt3a (50ng/ml) or Dkk-1 (100ng/ml) for 12hr and analyzed for *AXIN2* qRT-PCR. **m**, Downregulation of Wnt/ β -catenin signaling by shTMEM9 independently of Wnt ligand secretion. After transfection, cells were incubated with IWP-2 (2 μ M) for 12hr, and *AXIN2* expression was analyzed by qRT-PCR. **n**, Upregulated APC protein by TMEM9 depletion. *TMEM9* WT and KO cells analyzed by IF staining. GFP-expression marks shTMEM9-transduced cells (green dotted line). Experiments were performed three times with similar results.

Representative images of three independent experiments with similar results; Scale bars=20 μ m; NS: Not significant; Error bars: mean \pm S.D.; Two-sided unpaired *t*-test.



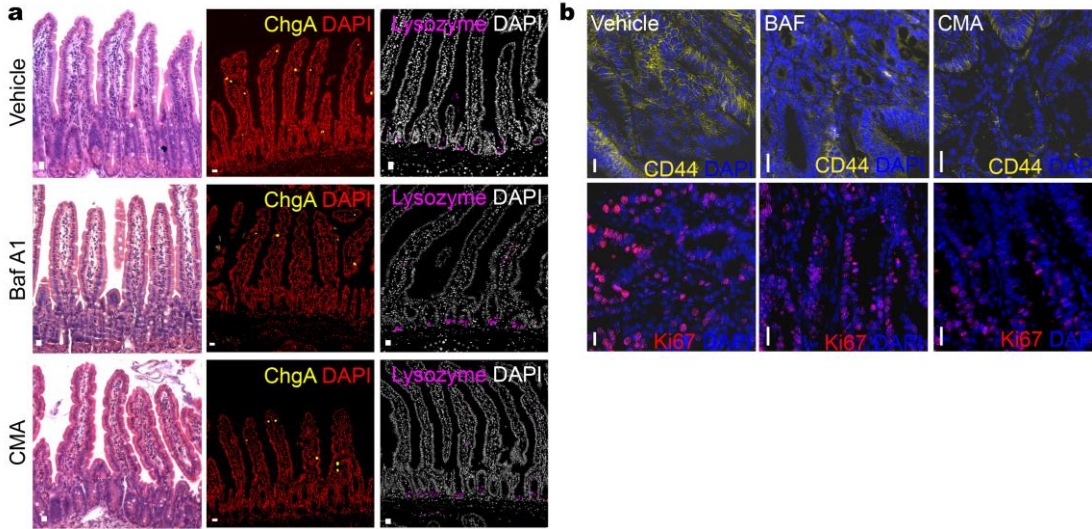
Supplementary Figure 4

Suppression of intestinal tumorigenesis by blockade of TMEM9

a, Correlation of TMEM9 expression with low survival in human CRC. The Kaplan–Meier plot of CRC specimens demonstrates significant (log-rank test) lower survival with TMEM9-high expression. Plots were analyzed from PrognScan, a publicly available

database (www.prognoscan.org). pmin: parallel minima, pcor: partial correlation. **b and c**, Transactivation of *TMEM9* by Wnt/ β -Catenin signaling. *TMEM9* is required for CRC cell proliferation (**b**). Each CRC cell line (shCtrl vs. sh*TMEM9*) was analyzed for cell proliferation by cell counting. IF staining of HCT116 (shCtrl and sh*TMEM9*; **c**) for Ki67. Experiments were performed three times with similar results. **d-f**, Reduced CRC cell proliferation by *TMEM9* depletion *ex vivo*. Each mouse (n=4 biologically independent samples) was subcutaneously injected with 1×10^7 cells into the left flank (HT29 [control]) and the right flanks (*TMEM9* KO-HT29). 15 days after transplantation, tumors were harvested for tumor assessment (**d**; n=4 mice). HCT116 cells were subcutaneously injected into immunocompromised mice. 28 days later, tumors were collected for imaging and weight analyses (**e**; n=8 mice). IF analyses of *TMEM9*-depleted tumors from xenograft (Ki67, CD44; **f**). **g**, The targeting strategy of *TMEM9* KO mouse model. **h**, No defects in the Paneth cell differentiation by *TMEM9* KO. IHC analysis of Lysozyme, a marker of Paneth cells, was performed in *TMEM9* KO mouse. **i**, Median survival of *APC*^{MIN}, *APC*^{MIN}:*TMEM9*^{+/-}, and *APC*^{MIN}:*TMEM9*^{-/-} mice. **j-m**, Suppression of intestinal tumorigenesis by *TMEM9* KO. Cyclin D1 IHC of small intestine samples from *APC*^{MIN}, *APC*^{MIN}:*TMEM9*^{+/-}, and *APC*^{MIN}:*TMEM9*^{-/-} mice (**j**). No alteration of cell death in *APC*^{MIN} and *APC*^{MIN}:*TMEM9*^{-/-} tumors. IHC of cleaved caspase-3 (c-Cas3; **k**). EMT marker analysis of *APC*^{MIN} and *APC*^{MIN}:*TMEM9*^{-/-} small intestine tumors. Markers of mesenchymal cell (N-cadherin and Vimentin) were not detected in tumors of both strains. The staining results of the mesenchymal cell in the *APC*^{MIN} normal intestine served as a positive control. DAPI was stained for the nuclei. No increase in cell death by *TMEM9* KO *in vivo* (**l**). No change in E-cadherin expression in *APC*^{MIN} and *APC*^{MIN}:*TMEM9* KO adenomas (**m**). E-cadherin expression was monitored by Super Resolution Level-Confocal Microscope (LSM880-Airyscan).

Representative images of three independent experiments with similar results; Scale bars=20 μ m; NS: Not significant; Error bars: \pm S.D. except for s5e (\pm S.E.M); Two-sided unpaired *t*-test. Centre: Average.

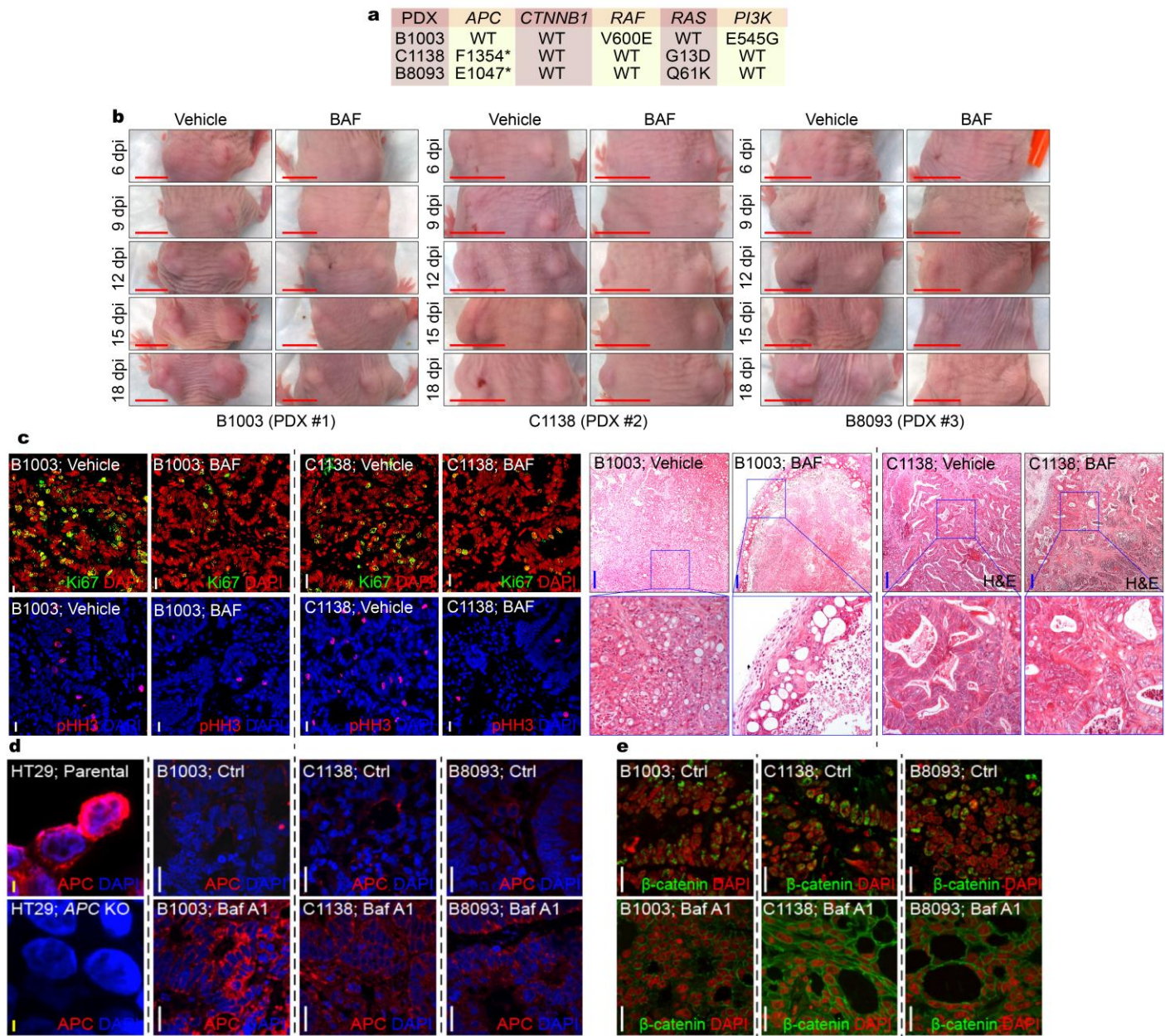


Supplementary Figure 5

Suppression of intestinal tumorigenesis by v-ATPase inhibitors

a, No defects in IEC differentiation by v-ATPase inhibitors. IHC for Chromogranin A (ChgA), a marker for the enteroendocrine cells, and Lysozyme, a marker for the Paneth cells in the non-tumor region of *APC^{MIN}* mice treated with v-ATPase inhibitors. **b**, Reduced CD44 expression and tumor cell growth by v-ATPase inhibitors. IHC for CD44 and Ki67.

Representative images of three independent experiments with similar results; Scale bars=20µm.



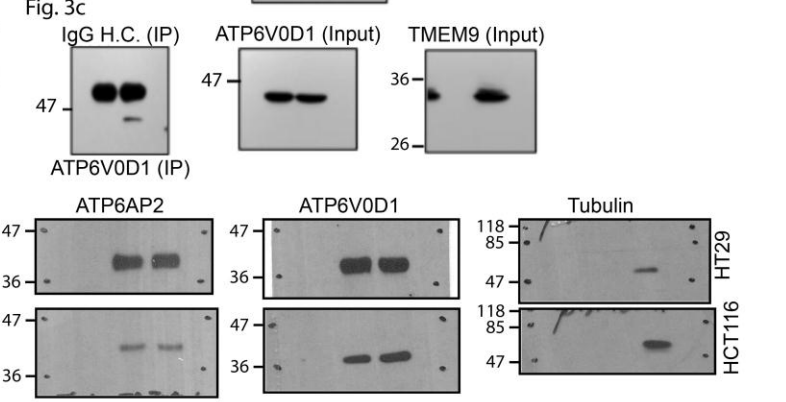
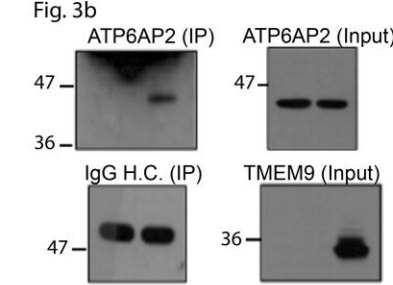
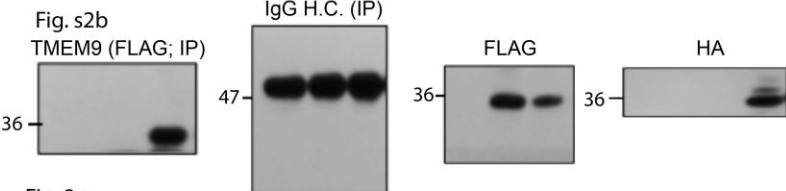
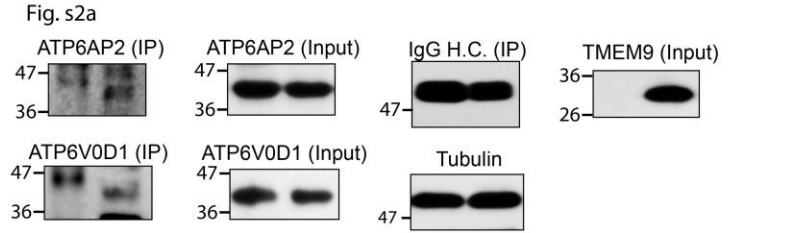
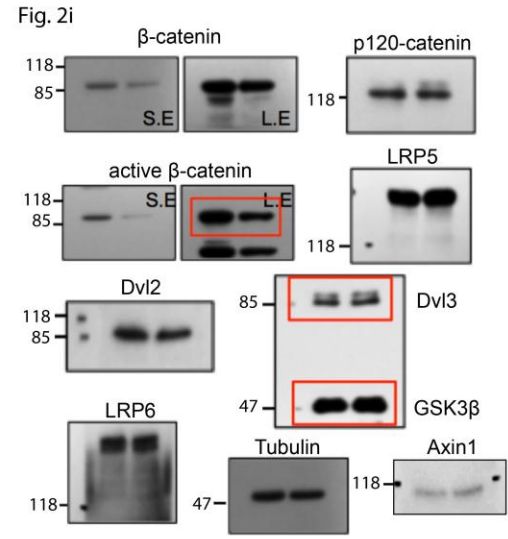
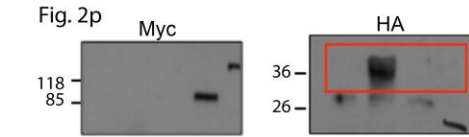
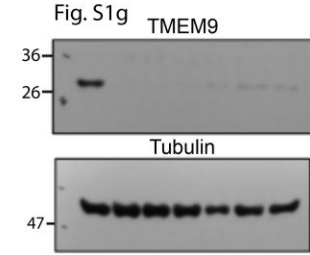
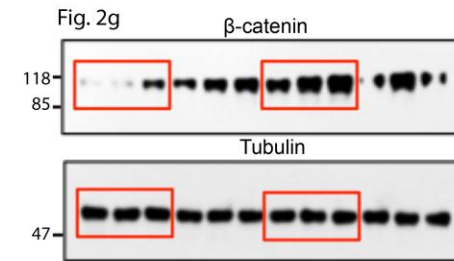
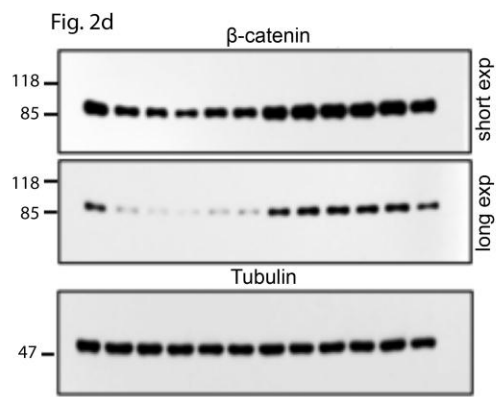
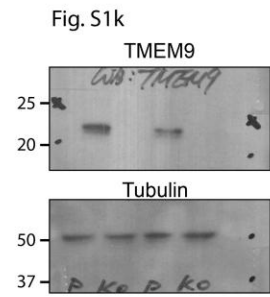
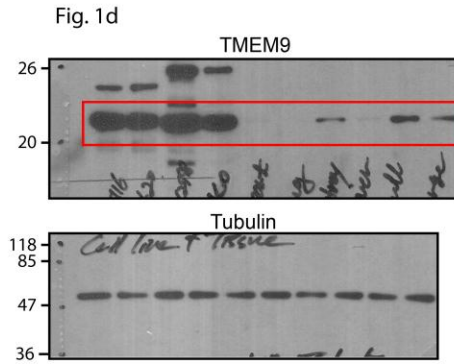
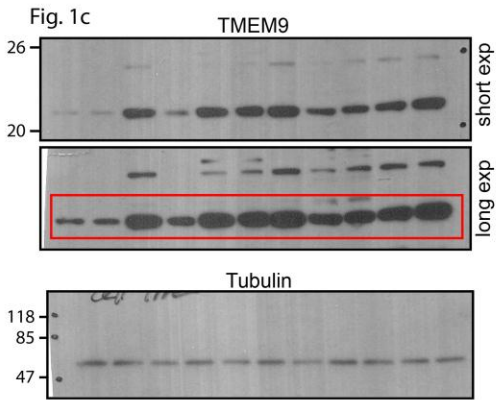
Supplementary Figure 6

Decreased PDX growth by v-ATPase inhibitor

a, Mutation status of PDXs. **b**, Suppression of PDX growth by BAF. Immunocompromised mice (BALB/c nude) were subcutaneously transplanted with three different CRC tissues from the patients into both right and left flanks. 7 days after transplantation, mice were injected with vehicle (corn oil) or BAF (1mg/kg and 3mg/kg) every 3 days for 15 days. At 18 days post-injection, CRC samples were collected for quantification. Experiment was performed once. **c**, Decreased cell proliferation by BAF in PDXs. IHC for phosphorylated-Histone H3 (pHH3; a marker of mitosis) and Ki67 (a marker of proliferative cells), and H&E. **d**, Increased APC expression by BAF. HT29-parental and HT29-APC KO cells served as a positive and negative control for IF staining of APC, respectively. BAF-treated PDXs displays the increased expression of APC protein. **e**, Redistribution of β -catenin by BAF. BAF-treated PDXs exhibited the redistribution of β -catenin protein mainly in the cytosol and cell-cell adhesion, whereas control PDXs showed the nuclear localization of β -catenin.

Representative images of three independent experiments with similar results; White scale bars=20 μ m; Blue scale bars=200 μ m; Red scale bars=1cm.

Scanned WB #1

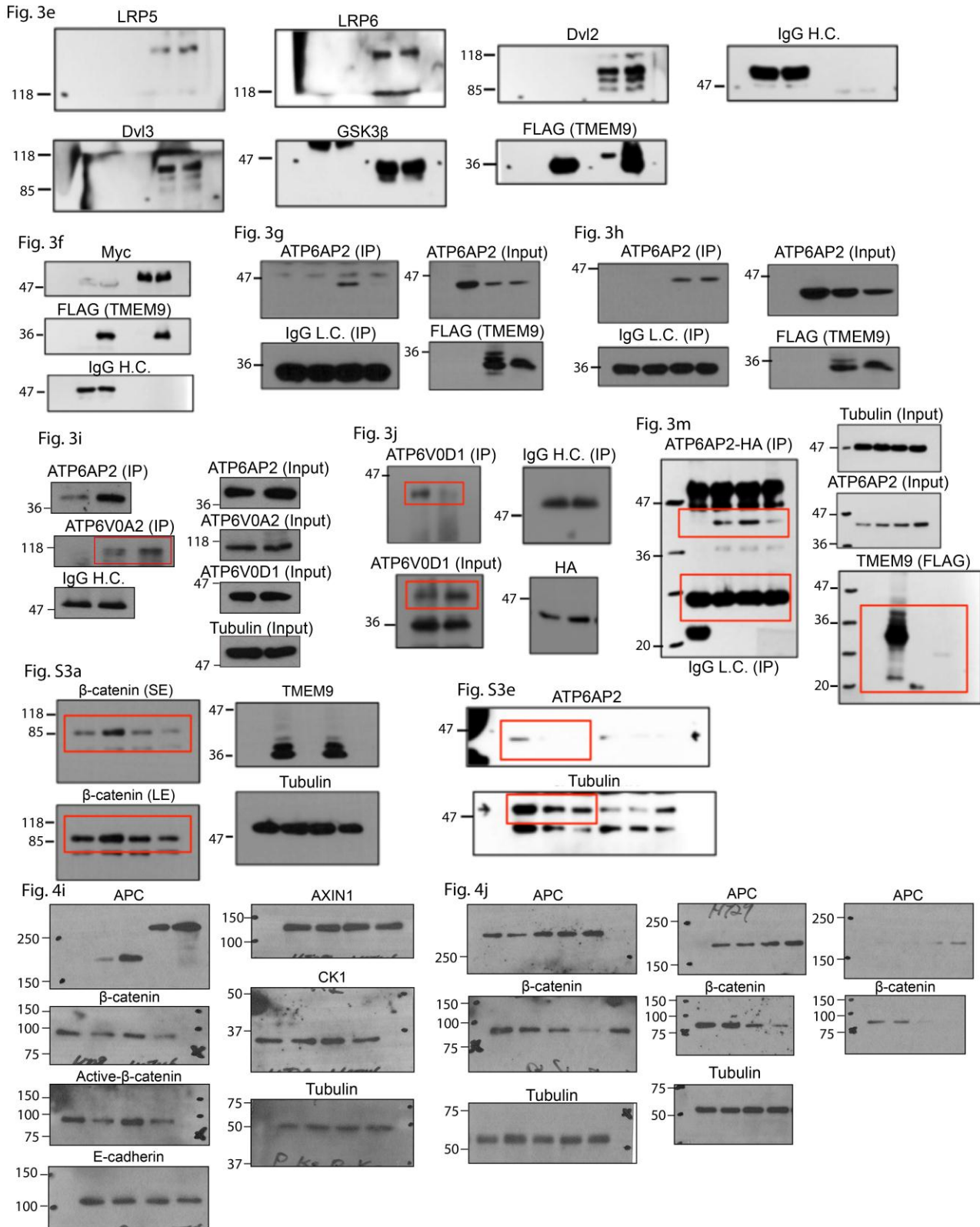


Supplementary Figure 7 (for page 1)

Unprocessed blots #1

Figs. 1c-3d

Scanned WB #2

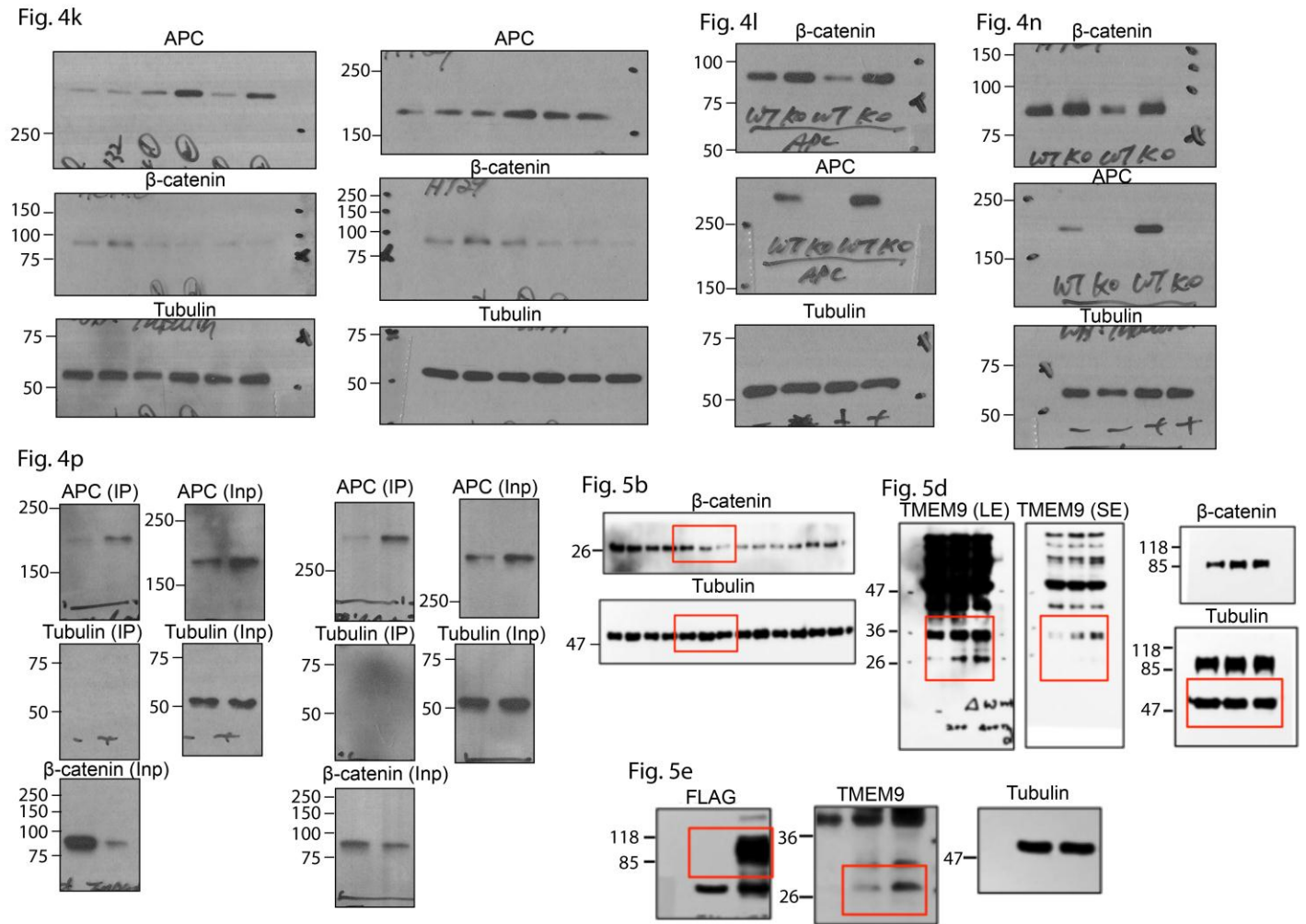


Supplementary Figure 7, continued (for page 2)

Unprocessed blots #2

Figs. 3e-4j

scanned WB #3



Supplementary Figure 7, continued (for page e)

Unprocessed blots #3

Figs. 4k-5e

Supplementary Table 1 List of genes highly expressed in CRC

To identify genes highly expressed in CRC, we used Oncomine (www.oncomine.org) datasets (fold change ≥ 2 ; $P < 0.0001$; gene rank $<$ top 5% upregulation). The table shows the list of increased genes in CRC including *TMEM9*.

Supplementary Table 2 Primer information

A complete list of primers.

Supplementary Table 3 Antibody information

A complete list of antibodies.

Supplementary Table 4 Statistics Source Data

11 sheets contain statistics source data.

Reporting Summary

Nature Research wishes to improve the reproducibility of the work that we publish. This form provides structure for consistency and transparency in reporting. For further information on Nature Research policies, see [Authors & Referees](#) and the [Editorial Policy Checklist](#).

Statistical parameters

When statistical analyses are reported, confirm that the following items are present in the relevant location (e.g. figure legend, table legend, main text, or Methods section).

n/a Confirmed

- The exact sample size (n) for each experimental group/condition, given as a discrete number and unit of measurement
- An indication of whether measurements were taken from distinct samples or whether the same sample was measured repeatedly
- The statistical test(s) used AND whether they are one- or two-sided
Only common tests should be described solely by name; describe more complex techniques in the Methods section.
- A description of all covariates tested
- A description of any assumptions or corrections, such as tests of normality and adjustment for multiple comparisons
- A full description of the statistics including central tendency (e.g. means) or other basic estimates (e.g. regression coefficient) AND variation (e.g. standard deviation) or associated estimates of uncertainty (e.g. confidence intervals)
- For null hypothesis testing, the test statistic (e.g. F , t , r) with confidence intervals, effect sizes, degrees of freedom and P value noted
Give P values as exact values whenever suitable.
- For Bayesian analysis, information on the choice of priors and Markov chain Monte Carlo settings
- For hierarchical and complex designs, identification of the appropriate level for tests and full reporting of outcomes
- Estimates of effect sizes (e.g. Cohen's d , Pearson's r), indicating how they were calculated
- Clearly defined error bars
State explicitly what error bars represent (e.g. SD, SE, CI)

Our web collection on [statistics for biologists](#) may be useful.

Software and code

Policy information about [availability of computer code](#)

Data collection	No software was used for data collection.
Data analysis	The human IPI databases version 3.6 (determination of peptide sequences) and SEQUEST ver.28 (fragmentation patterning) are used for analysis of mass spectrometry result. All statistical analyses and plots were generated using Graphpad Prism 7. Correlation analysis and heatmap were generated with the Graphpad Prism 7. Correlation analysis was conducted in Exel. Images were analyzed using AxioVision, ImageJ, and Zen software.

For manuscripts utilizing custom algorithms or software that are central to the research but not yet described in published literature, software must be made available to editors/reviewers upon request. We strongly encourage code deposition in a community repository (e.g. GitHub). See the Nature Research [guidelines for submitting code & software](#) for further information.

Data

Policy information about [availability of data](#)

All manuscripts must include a [data availability statement](#). This statement should provide the following information, where applicable:

- Accession codes, unique identifiers, or web links for publicly available datasets
- A list of figures that have associated raw data
- A description of any restrictions on data availability

Microarray data that support the findings of this study have been deposited in the Gene Expression Omnibus (GEO) under accession code GDS2947. The TMEM9 expression data in CRC cells were derived from the cBioportal using the TCGA Research Network: <http://cancergenome.nih.gov/> and Genetech datasets. The dataset derived from this resource that supports the findings of this study is available in OncoPrint (<https://www.oncoprint.org/resource>). TMEM9 expression data were also derived from cBioportal (<http://www.cbioportal.org/>) and COSMIC database (Catalogue of Somatic Mutations in Cancer) (<https://cancer.sanger.ac.uk/cosmic>). Source data for Figs. 1-8 and Supplementary Figs. 1-4 have been provided as Supplementary Table 4. All other data supporting the findings of this study are available from the corresponding author on reasonable request.

Field-specific reporting

Please select the best fit for your research. If you are not sure, read the appropriate sections before making your selection.

- Life sciences Behavioural & social sciences Ecological, evolutionary & environmental sciences

For a reference copy of the document with all sections, see nature.com/authors/policies/ReportingSummary-flat.pdf

Life sciences study design

All studies must disclose on these points even when the disclosure is negative.

Sample size	For animal studies, sample size was estimated by power calculation, as following; Using StatsToDo software (http://www.statstodo.com/SSiz2Means_Pgm.php ; alpha level P=0.05; power 80%; expected background standard deviation=0.5; difference between two means to be detected=0.5).
Data exclusions	No samples or animals were excluded. Also, the criteria were not pre-established in experiments.
Replication	All experiments were performed using at least three biological replicas unless specified. All experiments were successfully replicated.
Randomization	Tumor-bearing and genetic engineered animals in tumorigenesis studies were examined in certain aged groups (3-12 months of age) for determine the tumor suppressive effect and survival rate.
Blinding	Yes. Blinding was used for all analyses.

Reporting for specific materials, systems and methods

Materials & experimental systems

- | | |
|-------------------------------------|---|
| n/a | Included in the study |
| <input checked="" type="checkbox"/> | <input type="checkbox"/> Unique biological materials |
| <input type="checkbox"/> | <input checked="" type="checkbox"/> Antibodies |
| <input type="checkbox"/> | <input checked="" type="checkbox"/> Eukaryotic cell lines |
| <input checked="" type="checkbox"/> | <input type="checkbox"/> Palaeontology |
| <input type="checkbox"/> | <input checked="" type="checkbox"/> Animals and other organisms |
| <input type="checkbox"/> | <input checked="" type="checkbox"/> Human research participants |

Methods

- | | |
|-------------------------------------|---|
| n/a | Included in the study |
| <input checked="" type="checkbox"/> | <input type="checkbox"/> ChIP-seq |
| <input checked="" type="checkbox"/> | <input type="checkbox"/> Flow cytometry |
| <input checked="" type="checkbox"/> | <input type="checkbox"/> MRI-based neuroimaging |

Antibodies

Antibodies used

Active- β -catenin (Millipore; 8E7; 05-665)
 AIF (Cell signaling; D39D2; #5318)
 APC (Abcam; Ali 12-28; ab58)
 APC (Cell signaling; #2504)
 APC (NOVUS; NB100-91662)

ATP6AP2 (Abcam; ab40790)
 ATP6VOA2 (Thermo; PA5-22099)
 ATP6V0D1 (Santa Cruz; 34-Z; sc-81887)
 Axin1 (Cell signaling; C76H11; #2087)
 β -catenin (Cell Signaling; D10A8; #8480)
 CD44 (BD Bioscience; G44-26; 559942)
 Chromogranin A (Abcam; ab15160)
 CK1 (Cell signaling; #2655)
 cleaved caspase 3 (Cell signaling; 5A1E; #9664)
 Cyclin D1 (Cell Signaling; 92G2; #2978)
 Dvl2 (Cell signaling; 30D2; #3224)
 Dvl3 (Cell signaling; #3218)
 E-Cadherin (BD Bioscience; 36/N-Cadherin; 610182)
 EEA1 (Cell signaling; C45B10; #3288)
 FLAG (Sigma Aldrich; M2; F1804)
 GSK3 β (BD Bioscience; 7/GSK-3b; 610201)
 HA (Roche; 3F10; 11867423001)
 Ki67 (Cell Signaling; 8D5; #9449)
 LAMP1 (Cell signaling; D2D11; #9091)
 LRP5 (Cell signaling; D80F2; #5731)
 LRP6 (Cell signaling; C47E12; #3395)
 Lysozyme (Abcam; EPR2994(2); ab108508)
 Myc (Cell signaling; D84C12; #5605)
 N-Cadherin (BD Bioscience; 32/N-Cadherin; 610921)
 p120-catenin (Cell Signaling; #4989)
 phospho Histone H3 (Cell signaling; 6G3; #9706)
 RCAS1 (Cell signaling; D2B6N; #12290)
 TMEM9 (Abcam; ab82770 & Sigma; SAB2102477)
 Tubulin (Santa Cruz; D-10; sc-5274)
 Vimentin (BD Bioscience; RV202; 550513)

Validation

All antibodies used were validated by the respective commercial source for the application used in this manuscript.

Eukaryotic cell lines

Policy information about [cell lines](#)

Cell line source(s)

All cell lines were purchased from American Type Culture Collection (ATCC). KM12, HCT15, HT29, HCT116, COLO205, SW620, HCC2998, Hela, and 293T cells were maintained in Dulbecco's modified Eagle's medium (DMEM; Corning; 10-013-CV) containing 10% fetal bovine serum (FBS; Hyclone; SH3.007.003). FHC cell was maintained in DMEM: F-12 (Invitrogen; 11330-032) containing 10% FBS, cholera toxin (10ng/ml; Sigma; C-8052), insulin (5 μ g/ml; Sigma; I-1882), transferrin (5 μ g/ml; Fisher; 354204), and hydrocortisone (100ng/ml; Sigma; H-0008). CCD-841CoN, LS-174T, and RKO cells were maintained in Eagle's Minimum Essential Medium (EMEM; ATCC; 30-2003) containing 10% FBS. DLD-1 and NCI-H508 cells were maintained RPMI1640 (Corning; 10-049-CMR) containing 10% FBS. Mycoplasma contamination was examined using MycoAlert mycoplasma detection kit (Lonza; LT07-218).

Authentication

None of the cell lines were authenticated.

Mycoplasma contamination

All cell lines tested were negative for mycoplasma contamination

Commonly misidentified lines
(See [ICLAC](#) register)

No commonly misidentified lines were used.

Animals and other organisms

Policy information about [studies involving animals](#); [ARRIVE guidelines](#) recommended for reporting animal research

Laboratory animals

C57BL/6 mice (wildtype, APCmin, and TMEM9 KO): both gender, 3-12months of age, determination of tumorigenesis and survival rate.
 BALB/c nude mice: male, 4 months of age, xenograft, PDX.

Wild animals

The study did not involve wild animals.

Field-collected samples

The study did not involve field-collected samples.

Human research participants

Policy information about [studies involving human research participants](#)

Population characteristics

Patient 1: ID B1003, 84 years, female white T1N1M0 CRC, tissue collected: liver metastasis, treatment history: brief adjuvant trial of capecitabine (x3 weeks), poorly tolerated; 7 months prior to recurrence. Biopsy--Then 4 cycles of 5-FU + oxaliplatin + bev till PD --5FU+Irinotecan+ Cetuximab -- palliative radiation to inguinal LN-- 2 cycles of reduced-dose cetuximab--> deceased.

Characteristics: MSI-high. Kras: wt, BRAF:V600E, PIrCA: E545G, NRAS: no mut.

Patient 2: ID B8093, 31 years, female with white T4N1M1 CRC, tissue collected: LN metastasis; lung LN, treatment history: FOLFOX/Bev 7 cycles followed by radiation 2 years before this biopsy. Then found liver mets and received FOLFOX/Bev. Found to have new lung mets and received FOLFIRI/Bev for 3 months. Then, trametinib/palbociclib trial for 14 months. New brain met and got gamma-knife. Then reinitiated FOLFIRI/Bev for 6 months and found new brain met and breast mets, received palliative radiation -> --> deceased, Characteristics: MSS, Kras: wt, BRAF:no mutation, PIrCA: no mutation, NRAS: Q61K.

Patient 3: ID C1138, 32 years, female with white T3N1M1 CRC, tissue collected: liver metastasis, treatment history: outside laparoscopic showed T3N1M1 with liver met. Then started FOLFIRI+avastin for 3 months. Then 1st and 2nd stage hepatectomies. After 4 months found to have new liver mets and resumed FOLFIRI+avastin for 2 months. Then had new lung and bone mets. Enrolled to moonshot vaccine trial for 2 months then got PD. Reinitiated on FOLFIRI for 3 months and PD.-> --> deceased, Characteristics: MSS, Kras: G13D, BRAF:no mutation, PIrCA: no mutation, NRAS: no mutation.

Recruitment

Patients enrolled in the study were treated at The University of Texas MD Anderson Cancer Center. Patient tumor tissues and data were collected under an Institutional Review Board-approved protocol and an informed consent obtained from each patient.